

Simple deterministic dynamical systems with fractal diffusion coefficients

R. Klages^{1,*}, J.R. Dorfman²

¹*Institut für Theoretische Physik, Technische Universität Berlin, Hardenbergstraße 36, D-10623 Berlin, Germany; e-mail:R.Klages@physik.tu-berlin.de*

²*Institute for Physical Science and Technology and Department of Physics, University of Maryland, College Park, MD 20742, USA; e-mail: jrd@ipst.umd.edu*

(November 13, 2018)

We analyze a simple model of deterministic diffusion. The model consists of a one-dimensional periodic array of scatterers in which point particles move from cell to cell as defined by a piecewise linear map. The microscopic chaotic scattering process of the map can be changed by a control parameter. This induces a parameter dependence for the macroscopic diffusion coefficient. We calculate the diffusion coefficient and the largest eigenmodes of the system by using Markov partitions and by solving the eigenvalue problems of respective topological transition matrices. For different boundary conditions we find that the largest eigenmodes of the map match to the ones of the simple phenomenological diffusion equation. Our main result is that the diffusion coefficient exhibits a fractal structure by varying the system parameter. To understand the origin of this fractal structure, we give qualitative and quantitative arguments. These arguments relate the sequence of oscillations in the strength of the parameter-dependent diffusion coefficient to the microscopic coupling of the single scatterers which changes by varying the control parameter.

PACS numbers: 02.50.-r,05.40.+j,05.45.+b,05.60.+w,47.52.+j,47.53.+n

I. INTRODUCTION

Over the past years there has been a rapidly growing interest in trying to understand the mechanism of nonequilibrium transport on the basis of dynamical systems theory [1–9]. One line of work is related to computer simulations, where interacting many-particle systems under nonequilibrium conditions, like shear or an external field, are in the center of the investigations [10–14]. Another line of research focuses on low-dimensional models like the random [15–18] or periodic [19–31] Lorentz gas. An even simpler model which shares certain properties of the periodic Lorentz gas are two-dimensional multibaker maps [32–39]. Lorentz gases and multibaker maps have become standard models in the field of chaos and transport, since, on the one hand, they catch the physical essence of certain real nonequilibrium processes, but, on the other hand, they are still simple enough such that they can be analyzed in detail theoretically. The final point along this line of reduction of complexity is the problem of deterministic diffusion in one-dimensional maps, as it has first been studied by Grossmann and Fujisaka [40–42], by Geisel et al. [43–45], and by Schell, Fraser, and Kapral [46]. Later, methods of cycle expansion [47–51] and other techniques have been applied to this and related questions [52–56]. The most interesting problem in this context is to describe the dependence of deterministic diffusion on varying a single parameter value. However, for computing parameter-dependent diffusion coefficients so far either the deterministic dynamics could not be treated in full detail, and thus the results were approximative, or the task could be performed exactly only for a few simple cases of parameter values.

The idea of this article is to apply methods of dynamical systems theory, as discussed by Gaspard et al. [25,32,57], to the problem of parameter-dependent deterministic diffusion in one-dimensional piecewise linear maps. In the remaining part of this introductory section, we will explain the term deterministic diffusion, and we will define the class of dynamical system we want to analyze. In Section II, some important background of our approach will be discussed briefly, and in Section III, a method will be presented which enables the exact computation of deterministic diffusion coefficients for a broad range of parameter values. The result for the diffusion coefficient of the simple map considered here turns out to be surprisingly complex so that additional investigations, performed in Section IV, are required to understand the origin of this unexpected non-trivial diffusive behavior.

This article is based on the work of Ref. [58], Chapter 2, a brief summary has been published in Ref. [59].

A. What is deterministic diffusion?

In a first approach, one may think about diffusion as a simple non-correlated *random walk* [60–63], as sketched in Fig. 1: One starts by choosing an initial position x_0 of a point particle on the real line, e.g., $x_0 = 0$, as shown in the figure. The dynamics of the particle is then determined by fixing a probability density $\tilde{p}(s)$ such that $p(s) = \tilde{p}(s) ds$

gives the transition probability $p(s)$ for the particle to travel from its old position x_0 over a distance $s = x_1 - x_0$ to its new position x_1 . The same procedure can be applied to any further change in the position of the particle. For sake of simplicity, it is assumed that $\tilde{\rho}(s)$ is symmetric with respect to $s = 0$. The quantity of interest is here the orbit of the moving particle, which is represented by a collection of points $\{x_0, x_1, x_2, \dots, x_n\}$ on the real line. n refers to the discrete time, which is given by the number of iterations, or “jumps”, of the particle.

For performing a simple non-correlated random walk, it is assumed that the probability density $\tilde{\rho}(s)$ is independent of the position x_n of the particle and of the discrete time n , i.e., it is fixed in time and space. In other words, there is *no history* in the dynamics of the particle, that is, the single iteration steps are *statistically independent* from each other. This is called a *Markov process* in statistical physics [60,62,64]. Such a random walk can be used as a simple model for diffusion: One starts with an ensemble of particles at, e.g., $x_0 = 0$, and applies the iteration procedure introduced above to each particle. If one separates the real line into a number of subintervals of size Δx , the number n_p of particles in any such small interval after n iterations can be counted. Divided by the total number N_P of particles, these results determine the probability density $\rho_n(x)$ for a sufficiently large number of particles. This quantity can be interpreted as the probability to find one particle at a displacement x after n iterations. Thus, $\rho_n(x)$ provides information about the *macroscopic* distribution of an ensemble of particles, or of the average position of one particle, respectively. The diffusion coefficient D can now be obtained from the second moment of the probability density $\rho_n(x)$,

$$D = \lim_{n \rightarrow \infty} \frac{\langle x^2 \rangle}{2n} \quad , \quad (1)$$

where $\langle \dots \rangle := \int dx \rho_n(x) \dots$ represents the probability density average. If the probability densities are Gaussians, the diffusion coefficient of Eq. (1) is well-defined. This is the case for a *stochastic* diffusion process as the one modeled here by a simple random walk.

In contrast to this traditional picture of diffusion as an uncorrelated random walk, the theory of dynamical systems makes it possible to treat diffusion as a *deterministic dynamical process*: Here, the orbit of a point particle with initial condition x_0 may be generated by a *chaotic dynamical system*

$$x_{n+1} = M(x_n) \quad . \quad (2)$$

$M(x)$ is a one-dimensional map which determines how a particle gets mapped from position x_n to position x_{n+1} , as will be introduced in detail below. The map $M(x)$ plays now the role of the model-inherent probability density $\tilde{\rho}(s)$ of the previous random walk: Defining $M(x)$ together with Eq. (2) gives the full microscopic equations of motion of the system. Thus, the decisive new fact which distinguishes this dynamical process from the one of a simple uncorrelated random walk is that here x_{n+1} is *uniquely determined* by x_n rather than having a distribution of x_{n+1} for a given x_n . This way, the *complete history* of the particle is taken into account. If the resulting macroscopic process of an ensemble of particles, governed by a deterministic dynamical system like map $M(x)$, turns out to obey a law like Eq. (1), i.e., if a diffusion coefficient exists for the system, this process is denoted as *deterministic diffusion* [40–51].

B. The deterministic model

Fig. 2 shows the model which shall be studied in the following. This model has apparently first been introduced by Grossmann and Fujisaka [40,41]. It depicts a “chain of boxes” which continues periodically in both directions to infinity, and the orbit of a moving point particle. Let

$$M_a : \mathbb{R} \rightarrow \mathbb{R} \quad , \quad x_n \mapsto M_a(x_n) = x_{n+1} \quad , \quad a > 1 \quad , \quad x_n \in \mathbb{R} \quad , \quad n \in \mathbb{N}_0 \quad (3)$$

be a map modelling the chain of boxes introduced above, i.e., a *periodic continuation of discrete one-dimensional piecewise linear [65] expanding maps with uniform slope*. The index a denotes a control parameter, which is the absolute value of the slope of the map, x_n is the position of a point particle, and n labels the discrete time. Since the map is expanding, i.e. $a > 1$, its Lyapunov exponent $\ln a$ is greater than zero. Thus, $M_a(x)$ is dynamically unstable and may in this sense be called chaotic [66]. In order for the map to be chaotic and piecewise linear, it cannot be monotonic, so there must be points of discontinuity and/or non-differentiability. The term “chain” in the characterization of $M_a(x)$ can be made mathematically more precise as a *lift of degree one*,

$$M_a(x + 1) = M_a(x) + 1 \quad , \quad (4)$$

for which the acronym *old* has been introduced [67–69]. This means that $M_a(x)$ is to a certain extent translational invariant. Being *old*, the full map $M_a(x)$ is generated by the map of one box, e.g., on the unit interval $0 < x \leq 1$,

which will be referred to as the *box map*. It shall be assumed that the graph of this box map is point symmetric with respect to the center of the box at $(x, y) = (0.5, 0.5)$. This implies that the graph of the full map $M_a(x)$ is anti-symmetric with respect to $x = 0$,

$$M_a(x) = -M_a(-x) \quad , \quad (5)$$

so that there is no “drift” in the chain of boxes. For convenience, the class of maps defined by Eqs. (3), (4), and (5) shall be denoted as *class \mathcal{P}* (where \mathcal{P} stands for piecewise linear), and maps which fulfill the requirements of class \mathcal{P} shall be referred to as *class \mathcal{P} -maps*. In Fig. 2, which contains a section of a simple class \mathcal{P} -map, the box map has been chosen to

$$M_a(x) = \left\{ \begin{array}{ll} ax & , \quad 0 < x \leq \frac{1}{2} \\ ax + 1 - a & , \quad \frac{1}{2} < x \leq 1 \end{array} \right\} \quad , \quad a \geq 2 \quad , \quad (6)$$

cf. Refs. [40,57,66]. This example can be best classified as a *Lorenz map with escape* [70–74]. The chaotic dynamics of these maps is generated by a “stretch-split-merge”-mechanism for a density of points on the real line [71]. As a class \mathcal{P} -map, Eq.(6), together with Eqs.(3), (4), and (5), will be referred to as map \mathcal{L} . Other class \mathcal{P} -maps have been considered in Refs. [40,41,47,57,75,76], another example is discussed in Refs. [58,77,78].

It has been proposed [41] to look at the dynamics in this chain of boxes in analogy to the process of *Brownian motion* [60–62]: If a particle stays in a box for a few iterations, its *internal* box motion is supposed to get randomized and may resemble the microscopic fluctuations of a Brownian particle, whereas its *external* jumps between the boxes could be interpreted as sudden “kicks” the particle suffers by some strong collision. This suggests that “jumps between boxes” contribute most to the actual value of the diffusion coefficient. Brownian motion is usually described in statistical physics by introducing some stochasticity into the equations which model a diffusion process. The main advantage of the simple model discussed here is that diffusion can be treated by taking the full dynamics of the system into account, i.e., the *complete orbit* of the moving particle is considered, without any additional approximations. This is another way to understand the notion of deterministic diffusion in contrast to diffusion as obtained from stochastic approaches. That is, in the purely deterministic case the orbit of the particle is immediately fixed by determining its initial condition.

One should note that the strength of diffusion, and therefore the magnitude of the diffusion coefficient, are related to the probability of the particle to escape out of a box, i.e., to perform a jump into another box. This escape probability, however, as well as the average distance a particle travels by performing such a jump, changes by varying the system parameter. The problem which will be solved in the following is to develop a general method for computing parameter-dependent diffusion coefficients $D(a)$ for class \mathcal{P} -maps. Here, map \mathcal{L} will serve as a simple example. However, the methods to be presented should work as well for any other class \mathcal{P} -map, supposedly with analogous results (see, e.g., [58,77]).

II. FIRST PASSAGE METHOD

The methodology of first passage, as it has been developed in the framework of statistical physics [60,62], deals with the calculation of decay- or escape rates for ensembles of statistical systems with certain boundary conditions. In recent work by Gaspard et al., these methods have successfully been applied to the theory of dynamical systems [21,25,32,57,79,80]. In the following, the principles of first passage for the class \mathcal{P} of dynamical systems defined above will be briefly outlined. The method will turn out to provide a convenient starting point for computing parameter-dependent diffusion coefficients.

One may distinguish three different steps in applying the method:

Step 1: Solve the one-dimensional phenomenological *diffusion equation*

$$\frac{\partial n}{\partial t} = D \frac{\partial^2 n}{\partial x^2} \quad (7)$$

with suitable boundary conditions, where $n := n(x, t)$ stands for the macroscopic density of particles at point x and time t . This equation serves here as a *definition* for the diffusion coefficient D .

Step 2: Solve the *Frobenius-Perron equation*

$$\rho_{n+1}(x) = \int dy \rho_n(y) \delta(x - M_a(y)) \quad , \quad (8)$$

which represents the continuity equation for the probability density $\rho_n(x)$ of the dynamical system $M_a(y)$ [66,81].

Step 3: For a chain of boxes of chainlength L , consider the limit chainlength L and time n to infinity: If for given slope a the respective largest eigenmodes of n and ρ turn out to be identical in an appropriate scaling limit, then $D(a)$ can be computed by matching the eigenmodes of the probability density ρ to the particle density n : For *periodic boundary conditions*, i.e., $n(0, t) = n(L, t)$ and $\rho_n(0) = \rho_n(L)$, one obtains

$$D(a) = \lim_{L \rightarrow \infty} \left(\frac{L}{2\pi} \right)^2 \gamma_{dec}(a) \quad , \quad (9)$$

where $\gamma_{dec}(a)$ is the decay rate in the closed system to be calculated directly from the Frobenius-Perron equation and therefore determined by quantities of the deterministic dynamical system. For *absorbing boundary conditions*, i.e., $n(0, t) = n(L, t) = 0$ and $\rho_n(0) = \rho_n(L) = 0$, the same procedure leads to

$$D(a) = \lim_{L \rightarrow \infty} \left(\frac{L}{\pi} \right)^2 \gamma_{esc}(a) \quad , \quad (10)$$

where $\gamma_{esc}(a)$ is the escape rate for the open system. This quantity can be further determined by the escape rate formalism [9,82] to

$$\gamma_{esc}(a) = \lambda(\mathcal{R}; a) - h_{KS}(\mathcal{R}; a) \quad , \quad (11)$$

where the Lyapunov exponent $\lambda(\mathcal{R}; a)$ and the Kolmogorov-Sinai (KS) entropy $h_{KS}(\mathcal{R}; a)$ are defined on the repeller \mathcal{R} of the dynamical system. This equation is an extension of Pesin's formula to open systems, which is obtained in case of $\gamma_{esc} = 0$. Eqs.(9) and (10) have been applied to a variety of models, like the periodic Lorentz gas, two-dimensional multibaker maps and certain one-dimensional chains of maps, by Gaspard and coworkers [32,57]. Eq.(10), together with Eq.(11), has first been presented for the two-dimensional periodic Lorentz gas [21] and has later been generalized to other transport coefficients and dynamical systems [79,80]. However, although of fundamental physical importance, it seems in general to be difficult to use this equation for practical evaluations of $D(a)$, because usually the KS entropy is hard to calculate [66]. Instead, Eq.(10) with Eq.(11) can be inverted to get the KS entropy via the decay rate of the dynamical system of Eq.(9) to $h_{KS}(\mathcal{R}; a) = \lambda(\mathcal{R}; a) - \frac{1}{4}\gamma_{dec}(a)$ ($L \rightarrow \infty$) , or by employing Eq. (9) via the diffusion coefficient in the limit of large L .

III. SOLUTION OF THE FROBENIUS-PERRON EQUATION

Following the first passage method, the problem of computing parameter-dependent diffusion coefficients essentially reduces to solving the Frobenius-Perron equation for the dynamical system in a certain limit. In this section, a general method will be presented by which this goal can be achieved. Its principles will be illustrated by performing analytical calculations for some special cases of parameters of map \mathcal{L} . Our method is based on finding Markov partitions and on defining respective transition matrices. This approach is quite well-known, especially in the mathematical literature [83–90] and has been employed by many authors for the calculation of dynamical systems quantities [64,70,91–99]. We apply it here for the first time to compute the full parameter-dependent deterministic diffusion coefficient.

A. Transition matrix method

As a first example, the diffusion coefficient $D(a)$ shall be computed for map \mathcal{L} at slope $a = 4$, as sketched in Fig. 3, supplemented by periodic boundary conditions. The calculation will be done according to the three-step procedure outlined above.

Step 1: The one-dimensional diffusion equation Eq.(7) can be solved with periodic boundary conditions straightforward to

$$n(x, t) = a_0 + \sum_{m=1}^{\infty} \exp\left(-\left(\frac{2\pi m}{L}\right)^2 Dt\right) \left(a_m \cos\left(\frac{2\pi m}{L}x\right) + b_m \sin\left(\frac{2\pi m}{L}x\right) \right) \quad , \quad (12)$$

where a_0 , a_m and b_m are the Fourier coefficients to be determined by an initial particle density $n(x, 0)$.

Step 2: To solve the Frobenius-Perron equation, the key idea is to write this equation as a matrix equation [32,64]. For this purpose, one needs to find a suitable *partition* of the map, i.e., a decomposition of the real line into a set of

subintervals, called *elements*, or *parts* of the partition. The single parts of the partition have to be such that they do not overlap except at boundary points, which are referred to as *points of the partition*, and that they cover the real line completely [64]. In case of slope $a = 4$, such a partition is naturally provided by the box boundaries. The grid of dashed lines in Fig. 3 represents a two-dimensional image of the one-dimensional partition introduced above, which is generated by the application of the map.

Now an initial density of points shall be considered which covers, e.g., the interval in the second box of Fig. 3 uniformly. By applying the map, one observes that points of this interval get mapped two-fold on the interval in the second box again, but that there is also escape from this box which covers the third and the first box intervals, respectively. Since map \mathcal{L} is *old*, this mechanism applies to any box of the chain of chainlength L , modified only by the boundary conditions. Taking into account the stretching of the density by the slope a at each iteration, this leads to a matrix equation of

$$\boldsymbol{\rho}_{n+1} = \frac{1}{a} T(a) \boldsymbol{\rho}_n \quad , \quad (13)$$

where for $a = 4$ the $L \times L$ -transition matrix $T(4)$ can be constructed to

$$T(4) = \begin{pmatrix} 2 & 1 & 0 & 0 & \cdots & 0 & 0 & 1 \\ 1 & 2 & 1 & 0 & 0 & \cdots & 0 & 0 \\ 0 & 1 & 2 & 1 & 0 & 0 & \cdots & 0 \\ \vdots & & & \vdots & \vdots & & & \vdots \\ 0 & \cdots & 0 & 0 & 1 & 2 & 1 & 0 \\ 0 & 0 & \cdots & 0 & 0 & 1 & 2 & 1 \\ 1 & 0 & 0 & \cdots & 0 & 0 & 2 & 1 \end{pmatrix} . \quad (14)$$

The matrix elements in the upper right and lower left edges are due to periodic boundary conditions and reflect the motion of points from the L th box of the chain to the first one and *vice versa*.

In Eq.(13), the transition matrix $T(a)$ is applied to a column vector $\boldsymbol{\rho}_n$ of the probability density $\rho_n(x)$ which, in case of $a = 4$, can be written as

$$\boldsymbol{\rho}_n \equiv |\rho_n(x) \rangle := (\rho_n^1, \rho_n^2, \dots, \rho_n^k, \dots, \rho_n^L)^* \quad , \quad (15)$$

where “ $*$ ” denotes the transpose, and ρ_n^k represents the component of the probability density in the k th box, $\rho_n(x) = \rho_n^k$, $k - 1 < x \leq k$, $k = 1, \dots, L$, ρ_n^k being constant on each part of the partition.

In case of $a = 4$, the transition matrix is symmetric and can be diagonalized by spectral decomposition. Solving the eigenvalue problem

$$T(4) |\phi_m(x) \rangle = \chi_m(4) |\phi_m(x) \rangle \quad , \quad (16)$$

where $\chi_m(4)$ and $|\phi_m(x) \rangle$ are the eigenvalues and eigenvectors of $T(4)$, respectively, one obtains

$$\begin{aligned} |\rho_n(x) \rangle &= \frac{1}{4} \sum_{m=0}^{L-1} \chi_m(4) |\phi_m(x) \rangle \langle \phi_m(x) | \rho_n(x) \rangle \\ &= \sum_{m=0}^{L-1} \exp\left(-n \ln \frac{4}{\chi_m(4)}\right) |\phi_m(x) \rangle \langle \phi_m(x) | \rho_0(x) \rangle \quad , \end{aligned} \quad (17)$$

where $|\rho_0(x) \rangle$ is an initial probability density vector and $\ln 4$ is the Lyapunov exponent of the map. Note that the choice of initial probability densities is restricted by this method to functions which can be written in the vector form of Eq.(15). For matrices of the type of $T(4)$, it is well-known how to solve their eigenvalue problems [100–102]. This is performed in App. A 1 for a more general case, which includes the example under consideration. For slope $a = 4$, one gets

$$\begin{aligned} \chi_m(4) &= 2 + 2 \cos \theta_m \quad , \quad \theta_m := \frac{2\pi}{L} m \quad , \quad m = 0, \dots, L - 1 \quad ; \\ |\phi_m(x) \rangle &= (\phi_m^1, \phi_m^2, \dots, \phi_m^k, \dots, \phi_m^L)^* \quad , \quad \phi_m^k = \tilde{a}_m \phi_{m,1}^k + \tilde{b}_m \phi_{m,2}^k \quad , \\ \phi_{m,1}^k &:= \cos \theta_m (k - 1) \quad , \quad \phi_{m,2}^k := \sin \theta_m (k - 1) \quad , \\ k &= 1, \dots, L \quad , \quad k - 1 < x \leq k \end{aligned} \quad (18)$$

with \tilde{a}_m and \tilde{b}_m to be fixed by suitable normalization conditions.

Step 3: To compute the diffusion coefficient $D(4)$, it remains to match the first few largest eigenmodes of the diffusion equation to the ones of the Frobenius-Perron equation: In the limit as the time t and the system size L approach infinity, the particle density $n(x, t)$, Eq.(12), in the diffusion equation becomes

$$n(x, t) \simeq \text{const.} + \exp\left(-\left(\frac{2\pi}{L}\right)^2 Dt\right) \left(A \cos\left(\frac{2\pi}{L}x\right) + B \sin\left(\frac{2\pi}{L}x\right) \right) , \quad (19)$$

where the constant represents the uniform equilibrium density of the equation.

Analogously, for discrete time n and chainlength L to infinity, one obtains for the probability density $\rho_n(x)$ of the Frobenius-Perron equation, Eq.(17) with Eq.(18),

$$\rho_n(x) \simeq \text{const.} + \exp(-\gamma_{dec}(4)n) \left(\tilde{A} \cos\left(\frac{2\pi}{L}(k-1)\right) + \tilde{B} \sin\left(\frac{2\pi}{L}(k-1)\right) \right) , \quad (20)$$

$$k = 1, \dots, L \quad , \quad k-1 < x \leq k$$

with a decay rate of

$$\gamma_{dec}(4) = \ln \frac{4}{2 + 2 \cos \frac{2\pi}{L}} \quad (21)$$

of the dynamical system, determined by the second largest eigenvalue of the matrix $T(4)$, see Eq.(18). Note that the largest eigenvalue is equal to the slope of the map so that for the first term in Eq.(20) the exponential vanishes, and one obtains a uniform equilibrium density. Apart from generic discretization effects in the time and position variables, which may be neglected in the limit of time to infinity and after a suitable spatial coarse graining, the eigenmodes of Eqs.(19) and (20) match precisely so that, according to Eq.(9), the diffusion coefficient $D(4)$ can be computed to

$$D(4) = \left(\frac{L}{2\pi}\right)^2 \gamma_{dec}(4) = \frac{1}{4} + \mathcal{O}(L^{-4}) \quad . \quad (22)$$

This result is identical to what is obtained from a simple random walk model [46,58,78]. The procedure can be generalized straightforward to all even integers values of the slope, as is shown in App. A 1, and leads to a parameter-dependent diffusion coefficient of

$$D(a) = \frac{1}{24}(a-1)(a-2) \quad , \quad a = 2k \quad , \quad k \in \mathbb{N} \quad , \quad (23)$$

in agreement with results of Ref. [41].

A slightly more complicated example is the case of slope $a = 3$, see, e.g., Fig. 2, which will be treated in the following. Analogously to the previous example, for $a = 3$ a simple partition can be constructed, the parts of which are all of length $1/2$. According to this partition, a transition matrix $T(3)$ can be determined, given schematically by

$$T(3) = \begin{pmatrix} 1 & 1 & 0 & 0 & \cdots & 0 & 0 & 1 & 0 \\ 1 & 1 & 0 & 1 & 0 & 0 & \cdots & 0 & 0 \\ 1 & 0 & 1 & 1 & 0 & 0 & \cdots & 0 & 0 \\ 0 & 0 & 1 & 1 & 0 & 1 & 0 & 0 & \cdots \\ 0 & 0 & 1 & 0 & 1 & 1 & 0 & 0 & \cdots \\ \vdots & & \vdots & & & & \vdots & & \\ 0 & 1 & 0 & 0 & \cdots & 0 & 0 & 1 & 1 \end{pmatrix} . \quad (24)$$

Note that, in contrast to the case of $a = 4$, here the matrix is formed by submatrix *blocks* which move periodically to the right every two rows. Since the partition of $a = 3$ is a bit more complicated than for $a = 4$, the blocks refer to the partition of each box, whereas the shift again is related to the lift property of the *old* map. The matrix $T(3)$ is not symmetric. However, the eigenvalue problem of this matrix can still be solved analogously to the case of $a = 4$ (see App. A 1). The spectrum of the matrix turns out to be highly degenerate, and therefore $T(3)$ cannot be simply diagonalized anymore [103]. This is due to the fact that the matrix $T(3)$ is *non-normal*, i.e., $T(3)T^*(3) \neq T^*(3)T(3)$, which means that it does not provide a system of orthogonal eigenvectors. Of course still a transformation onto Jordan normal form to “block-diagonalize” this matrix could be applied. However, this seems to be more useful for proving mathematical theorems than for analytical calculations of diffusion coefficients [104]. Since the probability density of

the Frobenius-Perron equation is determined by iteration of transition matrices, cf. Eq. (13), for slope $a = 3$ it is not in advance clear how the single eigenmodes “mix” in the limit time and chainlength to infinity and whether they can be matched to the solutions of the diffusion equation as before so that the diffusion coefficient $D(3)$ is again simply determined by the second largest eigenvalue of the matrix.

This problem will first be approached pragmatically. Analogously to the analytical solutions of Eqs. (19) and (20) for slope $a = 4$, Fig. 4 shows a plot of the two second largest eigenmodes of $T(3)$ in comparison to the solution of the diffusion equation. Again, one observes total agreement, except differences in the fine structure. The same is true for the other first few largest eigenmodes of $T(3)$. Thus, although straightforward diagonalization and, therefore, a simple solution of the Frobenius-Perron equation like Eq. (17) are not possible anymore, the largest eigenmodes of $T(3)$ behave correctly in the sense of the phenomenological diffusion equation so that it is suggestive to compute the diffusion coefficient $D(3)$ via the second largest eigenvalue of $T(3)$ again. With

$$\gamma(3) = \ln \frac{3}{1 + 2 \cos(2\pi/L)} \quad , \quad (25)$$

see App. A 1, and Eq.(9), one gets

$$D(3) = \frac{1}{3} + \mathcal{O}(L^{-4}) \quad . \quad (26)$$

As for $a = 4$, this result is obtained as well from a simple random walk model. However, to produce this value, the respective random walk has to be defined in a slightly different way than for $a = 4$ [58,78]. Analogously to the case of even integer slopes, the exact calculations can be generalized to all odd integer values of the slope and lead to (see App. A 1)

$$D(a) = \frac{1}{24}(a^2 - 1) \quad , \quad a = 2k - 1 \quad , \quad k \in \mathbb{N} \quad , \quad (27)$$

which again is identical to the result of Ref. [41].

Before this approach will be extended to other parameter values of the slope in the following section, some details will be discussed which are closely related to the calculations above: A special feature of the diffusion coefficient results for integer slopes shall be pointed out; further limits of this method with respect to generalized diffusion coefficients shall be critically discussed; and the application of the method to absorbing boundary conditions shall be briefly outlined.

1. Diffusion coefficients for integer slopes

Eqs. (22) and (26) show already that $D(4) < D(3)$, which is at first sight counterintuitive. By evaluating the general formulas of $D(a)$ given by Eqs. (23) and (27) at other even and odd integer slopes, one realizes that this inequality reflects a general oscillatory behavior of $D(a)$ at integer slopes. This result has already been obtained by Fujisaka and Grossmann [41], but it has not been discussed in further detail in their work. A similar oscillatory behavior has been observed for deterministic diffusion in certain classes of two-dimensional maps [105–109]. This behavior cannot be understood completely by one consistent simple random walk model [58,78].

2. Matching lower eigenmodes

There appear serious problems in trying to extend the matching eigenmodes procedure to arbitrarily low eigenmodes, even in case of $a = 4$, where the matrix is diagonalizable. With Eq.(18), one can check that

$$\phi_{m,1}^k = \phi_{L-m,1}^k \quad , \quad \phi_{m,2}^k = -\phi_{L-m,2}^k \quad ; \quad k = 1, \dots, L \quad , \quad m = 1, \dots, L - 1 \quad , \quad (28)$$

i.e., in contrast to the m eigenmodes of the diffusion equation Eq.(7), the frequency of the eigenmodes of $T(4)$ does not increase monotonically with m , but gets “flipped over” at the $(L/2)$ th (for L even) eigenmode such that the first and the last half of the number of eigenmodes are identical, except a minus sign. This is due to the discretization of the position variable x in the diffusion equation to k in the Frobenius-Perron *matrix* equation Eq.(13), which was one of the basic ingredients for the possibility to construct transition matrices.

Moreover, one should note that, according to Eq.(18), the smallest eigenvalue of $T(4)$ is equal to zero. For $T(3)$, a large number of eigenvalues are even less than zero (see Eq. (A16) in App. A 1 for $a = 3$). Thus, except for the

first few largest eigenmodes, which still match reasonably well to the eigenmodes of the diffusion equation in the limit time n and chainlength L to infinity, one cannot expect the method to work simply that the components of a “time-dependent” diffusion coefficient $D_n(a)$ are determined by smaller eigenvalues of the transition matrices in straight analogy to Eq.(9). This could be taken as a hint that, to obtain more details of the dynamics, refined methods are needed. For example, in Ref. [110] the first orders of a position-dependent diffusion coefficient have been determined for a class \mathcal{P} -map according to a procedure which avoids the discretization of the real line.

3. Absorbing and periodic boundary conditions

The same procedure as outlined for periodic boundary conditions can also be employed for absorbing boundaries. It shall be sketched briefly, according to the three steps distinguished before:

Step 1: The one-dimensional diffusion equation with absorbing boundary conditions can be solved to

$$n(x, t) = \sum_{m=1}^{\infty} a_m \exp\left(-\left(\frac{\pi m}{L}\right)^2 Dt\right) \sin\left(\frac{\pi m}{L} x\right) \quad (29)$$

with a_m denoting again the Fourier coefficients.

Step 2: The transition matrices for $a = 4$ and $a = 3$ at these boundary conditions are identical to the ones of Eqs.(14),(24), except that the matrices now contain zeroes as matrix elements in the upper right and lower left corners. However, due to this slight change in their basic structure there is no general method to solve the eigenvalue problems for this type of matrices anymore, in contrast to the case of periodic boundary conditions. At least for $a = 3$ and $a = 4$, it is still possible to obtain analytical solutions by straightforward calculations analogous to the ones performed in Ref. [32] (see App. A 2), but for any higher integer value of the slope even these basic methods fail. This appears to be caused by strong boundary layers. Fig. 5 shows numerical solutions for the largest eigenmodes of the first odd integer slope transition matrices in comparison to the solutions of the diffusion equation Eq.(7) (details of the numerics applied here are given in the following section). It can be seen that near the boundaries, there are pronounced deviations between the Frobenius-Perron and the diffusion equation solutions. These deviations are getting smaller in the interior region of the chain, but are gradually getting stronger with increasing the value of the slope, as is shown in the magnification. The same behavior can be found for even integer slopes, although the quantitative deviation of these eigenmodes from the ones of the diffusion equation solutions is slightly less than for odd values of the slope. Thus, obviously absorbing boundary conditions disturb the deterministic dynamics significantly, whereas similar effects do not occur for periodic boundary conditions, which therefore could be characterized as a kind of “natural boundary conditions” for this periodic dynamical system.

Step 3: The different boundary conditions do not only show up in the eigenmodes of the transition matrices, but also in the calculation of the diffusion coefficients. In analogy to periodic boundary conditions, the escape rate of the dynamical system at $a = 3$ and $a = 4$ is determined to

$$\gamma_{esc}(a) = \ln \frac{a}{\chi_{max}(a)} \quad (30)$$

with $\chi_{max}(a)$ being the largest eigenvalue of the transition matrix (see App. A 2),

$$\chi_{max}(3) = 1 + 2 \cos \frac{\pi}{L+2} \quad \text{and} \quad \chi_{max}(4) = 2 + 2 \cos \frac{\pi}{L+1} \quad . \quad (31)$$

Feeding this into Eq.(10) via matching eigenmodes, one obtains

$$\begin{aligned} D(3) &\simeq \frac{1}{3} \frac{L^2}{(L+2)^2} + \mathcal{O}(L^{-4}) \rightarrow \frac{1}{3} \quad (L \rightarrow \infty) \quad , \\ D(4) &\simeq \frac{1}{4} \frac{L^2}{(L+1)^2} + \mathcal{O}(L^{-4}) \rightarrow \frac{1}{4} \quad (L \rightarrow \infty) \quad , \end{aligned} \quad (32)$$

which gives a convergence of the diffusion coefficient with the chainlength L significantly below that obtained from periodic boundary conditions. For example, for a chainlength of $L = 100$ the convergence is about two orders of magnitude worse. It can be concluded that the transition matrix method works in principle for absorbing boundary conditions as well, but that here its range of application to compute diffusion coefficients is qualitatively and quantitatively more restricted because of long-range boundary layers.

B. Markov partitions

In the previous section, the choice of simple partitions enabled the construction of transition matrices. These matrices provided a way to solve the Frobenius-Perron equation in a certain limit. However, so far this method has only been applied to very special cases of map \mathcal{L} , defined by integer slopes. This raises the question whether an extension of this method to other values of the slope is possible. For this purpose, the idea of choosing a suitable partition of the map has to be generalized. Taking a look at Fig. 3 again, one observes that the graph of the map “crosses” or “touches” a vertical line of the grid only at some grid points. Furthermore, the local extrema of the map, which are here identical to the points of discontinuity, are situated on, or just “touch” horizontal lines of the grid, whereas other crossovers of horizontal lines occur at no specific point. The same characteristics can be verified, e.g., for the respective partition of slope $a = 3$. These conditions ensure that it is possible to obtain a correct transition matrix from a partition, since to be modeled by a matrix, a density of points, which covers parts of the partition completely, has to get mapped in a way that its image again covers parts of the partition completely, and not partially. This basic property of a “suitable partition to construct transition matrices” is already the essence of what is known as a *Markov partition*:

Definition 1 (Markov partition, verbal definition) *For one-dimensional maps, a partition is a Markov partition if and only if parts of the partition get mapped again onto parts of the partition, or onto unions of parts of the partition [64].*

A more formal definition of one-dimensional Markov partitions, as well as further details, can be found in Refs. [87,90,111]. The next goal must be to find a general rule of how to construct Markov partitions for map \mathcal{L} at other, non-trivial parameter values of the slope. Because of the periodicity of the chain of maps it suffices to find a Markov partition for a single *box map*, i.e., for the respective map in one box without applying the modulus to restrict it onto the unit interval. Here, the fact can be used that the extrema, which are the *critical points* of the box map, have to touch horizontal lines, as explained before, which means that to obtain a Markov partition the extrema have to get mapped onto partition points. Since any box map of map \mathcal{L} is symmetric with respect to the point $(x, y) = (0.5, 0.5)$, the problem reduces to considering only one of the extrema in the following, e.g., the maximum. Changing the height of the maximum corresponds to changing the slope of the map. Therefore, if one needs to find Markov partitions for parameter values of the slope, one can do it the other way around by the following *Markov condition*:

Definition 2 (Markov condition, verbal definition) *For map \mathcal{L} , Markov partition values of the slope are determined by choosing the slope such that the maximum of the box map gets mapped onto a point of the partition again.*

In Fig. 6, four examples of non-trivial Markov partitions for map \mathcal{L} are depicted with respect to their box maps. One may check that the handwaving conditions which have been extracted from the integer slope examples to motivate Definition 1 are fulfilled and especially that the partitions shown in the figure obey the Markov partition definition 1. The detailed structure of the partitions can be arbitrarily complex. In Fig. 6 (a) and (b) a special orbit has been marked by bold black lines with arrows. It represents what will be called the *generating orbit* of a Markov partition: For the two examples shown here, the starting point of this orbit is given by the maximum of the preceding box map, since this maximum must also be a partition point. The iterations of this orbit, as indicated by the arrows in the figure, define the single partition points. This way, the number of partition parts is related to the number of iterations of the generating orbit. In case of Fig. 6 (a) and (b) the orbit is eventually periodic, i.e., it finally gets mapped onto the fixed point $x = 0$, however, it can also be periodic with a certain period, as, for example, in case of Fig. 6 (d) (period four). Thus, the generating orbit is the key of how to find Markov partition values of the slope in a systematic way.

On this basis, a general algebraic procedure to compute such values of the slope can be developed. One starts with a further *topological reduction* of the whole chain of boxes [112]. Since map \mathcal{L} is *old*, it is possible to construct the Markov partition for the whole chain from a *reduced map*

$$\tilde{M}_a(\tilde{x}) := M_a(\tilde{x}) \pmod{1} \quad (33)$$

via periodic continuation, where $\tilde{x} := x - [x]$ is the fractional part of x , $\tilde{x} \in (0, 1]$, and $[x]$ denotes the largest integer less than x . Therefore, it remains to find Markov partitions for map $\tilde{M}_a(\tilde{x})$ of the equation above. This can be done in the following way: Let

$$\epsilon := \min \left\{ \tilde{M}_a\left(\frac{1}{2}\right), 1 - \tilde{M}_a\left(\frac{1}{2}\right) \right\} \quad , \quad \epsilon \leq \frac{1}{2} \quad , \quad (34)$$

be the minimal distance of a maximum of the box map $M_a(\tilde{x})$ to an integer value. With respect to the Markov condition given by Definition 2, it is clear that ϵ has to be a partition point. Since $\tilde{M}_a(\tilde{x})$ is point symmetric, $1 - \epsilon$ also has to be a partition point, and because of map \mathcal{L} being *old*, the fixed point $x = 0$ is necessarily another partition point. Thus, the reduced map governs its internal box dynamics according to

$$\tilde{x}_{n+1} = \tilde{M}_a(\tilde{x}_n) \quad , \quad \tilde{x}_n = \tilde{M}_a^n(\tilde{x}) \quad , \quad \tilde{x} \equiv \tilde{x}_0 \quad . \quad (35)$$

Since $0, \epsilon$ and $1 - \epsilon$ have to be partition points, the Markov condition Definition 2 can be formalized to

$$\tilde{M}_a^n(\epsilon) \equiv \delta \quad , \quad \delta \in \{0, \epsilon, 1 - \epsilon\} \quad , \quad (36)$$

i.e., the generating orbit of a Markov partition is defined by the initial condition ϵ , its end point δ and the iteration number n . According to Eq.(34), ϵ is determined by the slope a . Therefore, for map \mathcal{L} Markov partition values of the slope can be computed as solutions of Eq.(36). The evaluation of this equation can be performed numerically as well as, to a certain degree, analytically. To obtain analytical results for Markov partition values of the slope, one has to determine the structure of the generating orbit in advance, i.e., one has to know whether it hits the left or the right branch of the box map at the next iteration. Then one can write down an algebraic equation which remains to be solved. For example, for the Markov partition Fig. 6 (c), the generating orbit is determined by

$$x_1 = \tilde{M}_a(\epsilon) \quad , \quad \epsilon \leq \frac{1}{2} \quad \text{and} \quad \delta \equiv \tilde{M}_a(x_1) - 3 \quad , \quad x_1 \leq \frac{1}{2} \quad (37)$$

with $a = 2(3 + \epsilon)$ and $\delta = 0$ at iteration number $n = 2$. This leads to

$$a^3 - 6a^2 - 6 = 0 \quad , \quad a \geq 2 \quad , \quad (38)$$

for which one may verify $a \simeq 6.158$ as the correct solution. This way, all Markov partition values of the slope are the roots of algebraic equations of $(n + 1)$ th order. More examples with analytical solutions are discussed in App. A 3. Since one usually faces the problem to solve algebraic equations of order greater than 3, numerical solutions of Eq.(36) are desirable, although one should take into account that iterations of the reduced map $\tilde{M}_a(\tilde{x})$ contain many discontinuities, due to the original discontinuity of $\tilde{M}_a(\tilde{x})$ at $\tilde{x} = 1/2$ as well as due to applying the modulus to $M_a(\tilde{x})$ in Eq.(33) [113].

With respect to the three different end points δ of the generating orbit in the formal Markov condition Eq.(36), three series of Markov partitions can be distinguished. For each series one can increase the iteration number n , and one can vary the range of the slope a systematically. These three series have been used as the basis for numerical calculations of the diffusion coefficient $D(a)$, as will be explained below. However, there exist additional suitable end points δ for the generating orbit. As an example, one can choose δ to be a point on a two-periodic orbit,

$$\tilde{M}_a^2(\delta) = \delta \quad , \quad a = 2(1 + \epsilon) \quad , \quad 0 \leq \epsilon \leq \frac{1}{2} \quad \Rightarrow \quad \delta = \frac{1 + 2\epsilon}{4(1 + \epsilon)^2 - 1} \quad (39)$$

so that the generating orbit is again eventually periodic, but now being mapped on a periodic orbit which is part of the Markov partition instead of being mapped on a simple fixed point. This way, certain periodic orbits can serve for defining an arbitrary number of new Markov partition series with respect to the choice of respective new end points δ . On the other hand, the set of Markov partition generating orbits is *not* equal to the set of *all* periodic orbits. For example, for the range $2 \leq a \leq 3$, Eq.(39) shows that there exists a two-periodic orbit for any slope a , but *not any* maximum of the map in this range necessarily maps onto this periodic orbit, as is already illustrated by Fig. 6 (a) and (b), or by other simple solutions of Eq.(36), respectively. This proves that Markov partition generating orbits are in fact a subset of all periodic orbits of the map.

With respect to varying the iteration number n and the end point δ , one can expect to get an infinite number of Markov partition values of the slope. In fact, for certain classes of maps the existence of Markov partitions can be considered as a natural property of the map [83,85,86,90]. According to the explanations above, this does not seem to be true for map \mathcal{L} . Instead, there is numerical evidence for the following conjecture [114]:

Conjecture 1 (Denseness property of Markov partitions) *For map \mathcal{L} , the Markov partition values of the slope are dense on the real line with $a \geq 2$.*

This denseness conjecture should ensure that it is possible to obtain a representative curve for the parameter-dependent diffusion coefficient $D(a)$ solely by computing diffusion coefficients at Markov partition values of the slope. Conjecture 1 may hold for all other class \mathcal{P} -maps as well. To do such computations, one needs to construct the corresponding

transition matrices to the Markov partitions obtained, as it has been shown for the slopes $a = 3$ and $a = 4$ of map \mathcal{L} . This can be done according to the following rule: Take as an example any of the box map Markov partitions illustrated in Fig. 6, e.g., case (a). Any dashed rectangle of this partition may be denoted as a *cell of the partition*. These single cells correspond to the single entries, or matrix elements, of the transition matrix to be obtained. The transition matrix corresponding to this Markov partition can now be constructed by checking where the graph of the map goes across a cell of the partition, by counting the number of these occurrences in each cell and by writing down these values as the matrix elements. For map \mathcal{L} , usually these matrix elements will consist of zeroes and ones, but the way they are defined here they can also take other integer values, depending on the choice of the partition, as, e.g., illustrated in case of $a = 4$, Eq. (11).

The construction of the box map transition matrix can be simplified by taking the point symmetry of the box map into account. The transition matrix of the full chain of chainlength L again follows by periodic continuation. These matrices can be denoted as *topological transition matrices*, since they reflect purely the topology of the map with respect to the Markov partitions, without involving any transition probabilities at this point. In Refs. [70,83,85,86,90] mathematically rigorous definitions of these transition matrices can be found. The property of map \mathcal{L} being *old* induces a certain structure in the topological transition matrices. They are said to be *banded square block Toeplitz matrices*, i.e., they consist of certain submatrices, called *blocks*, corresponding to the box map Markov partitions, and these blocks are the same along diagonals of the topological transition matrix parallel to the main diagonal, forming *bands* [102,115,116]. Applying periodic boundary conditions to the chain of boxes defines a subclass of these Toeplitz matrices, called *block circulants*, where each row is constructed by cycling the previous row forward one block [100–102,115], see, e.g., the matrices $T(4)$, Eq.(14), as an example for a simple circulant and $T(3)$, Eq.(24), for a block circulant. According to the transition matrix method outlined in the previous section, it remains to solve the eigenvalue problems of these matrices and to match the respective eigenmodes to the ones of the diffusion equation for computing the corresponding diffusion coefficients $D(a)$. Here, periodic boundary conditions are of great advantage. Analytically, as mentioned before and as shown in App. A 1, there exists a general procedure how to solve the eigenvalue problems of simple circulants [100–102], and in some cases it is possible to reduce the eigenvalue problem of a block circulant to that of a simple circulant (see App. A 1 and A 3). If this method works, it automatically yields “nice eigenmodes”, i.e., eigenvectors of the form of sines and cosines with some fine structure. These eigenmodes are similar to the eigenmodes of the diffusion equation at this stage (see App. A 3), i.e., before iterating the matrices according to the Frobenius-Perron matrix equation Eq.(13). The situation is quite different for absorbing boundary conditions, where no such general procedure exists (see App. A 2).

If analytical solutions of the eigenvalue problems are not possible anymore, one can obtain numerical solutions. Well-known software packages like NAG and IMSL provide subroutines to solve the eigenvalue problems of these matrices. Unfortunately, the numerically obtained results for the full spectra turned out not to be very reliable to a certain extent: In comparison to analytical results for periodic boundaries (see App. A 3), the NAG package does not compute all eigenvectors correctly, i.e., in the numerical results usually some linear independent eigenvectors are missing. Moreover, both packages provide spectra of eigenvalues which, although partly identical to the analytical solutions, differ in their full range quantitatively to the ones calculated analytically, not taking any degeneracy into account [117]. Such numerical problems seem to be inherent to the class of non-normal Toeplitz matrices, as has already been pointed out by Beam and Warming [115]. In fact, solving eigenvalue problems for Toeplitz matrices can be considered as a field of active recent research in numerical mathematics [118,119]. However, solely for the purpose of computing diffusion coefficients not the full spectra of the transition matrices are required, but only the few largest eigenvalues and eigenvectors are of interest. With respect to eigenvectors, the IMSL package has been checked to be reliable in this range, and with respect to eigenvalues, both packages provide exact and identical numerical results, especially for the second largest eigenvalue, which determines the diffusion coefficients. From a practical point of view, the NAG package is considerably more efficient in the use of computing time than IMSL and more flexible in its subroutines. Therefore, for quantitative computations of eigenvalues and diffusion coefficients NAG routines have been used, whereas for eigenvector computations IMSL procedures have been employed. For computations of diffusion coefficients, it is also favorable to consider only the case of periodic boundary conditions, i.e., solving eigenvalue problems for block circulants, respectively, since it has already been discussed in Sect III A that absorbing boundaries lead to a poor convergence rate of the diffusion coefficient with the chainlength L .

Fig. 7 contains two examples of second largest eigenmodes for chains of boxes with periodic boundaries and non-trivial Markov partitions. Again, one gets “nice” second largest eigenmodes, i.e., functions which behave like sines and cosines on a large scale. However, the structure of these eigenmodes is much more complex on a fine scale, as can be seen in the magnifications of certain regions. The periodic continuation of the fine structure suggests that it is related to the dynamics of the box map, and therefore varies with changing the slope, whereas the general large-scale behavior of the eigenmodes seems to be a property of the chain of boxes which shows up independently from such microscopic details. These characteristics have been checked numerically for a variety of other Markov partition values of the slope and seem to be a universal feature of map \mathcal{L} , and probably of all class \mathcal{P} -maps. One may assume

that the fine structure is somehow related to the strength of the diffusion coefficient and that, on the other hand, the universal large-scale structure of the eigenmodes is related to the existence of diffusion coefficients for non-trivial Markov partition values of the slope. In fact, the specific character of the eigenmodes discussed above, which shows up in any analytical solution of (block) circulants and which is supported by numerical results, forms the basis for the following conjecture:

Conjecture 2 (Existence of diffusion coefficients) *Let $M_a(x)$ be a class \mathcal{P} -map. If for given value of the slope the map is uniquely ergodic and if there exists a Markov partition, then the map is diffusive.*

To our knowledge, so far no proof has been given in the literature for the existence of diffusion coefficients in class \mathcal{P} -maps for general value of the slope. However, dealing with a rigorous foundation of the transition matrix method turns out to be intimately connected to proving the existence of diffusion coefficients in this class of dynamical systems. Without going into too much detail here, some remarks are in order to provide at least a motivation for this conjecture: The existence of Markov partitions guarantees that exact transition matrices can be used. The restriction to class \mathcal{P} -maps ensures that topological transition matrices can be constructed in the simple way outlined before, and the *old* property included in the definition of class \mathcal{P} determines the global structure of the topological transition matrices such that the eigenmodes are “nice”, at least for periodic boundary conditions. The requirement to be uniquely ergodic establishes the possibility of diffusion in the chain of boxes and confirms also the uniqueness of the diffusion coefficient to be obtained (a simple counterexample shows that not any chain of boxes with escape out of one box is automatically diffusive). Finally, the term diffusive shall be understood in the sense that a diffusion coefficient exists as defined by the statistical diffusion equation Eq.(7), which has been introduced to the dynamical system by successfully performing the matching eigenmodes procedure outlined in the previous section. Therefore, the main proposition of this conjecture is that the matching eigenmodes procedure required by the first passage method works for any value of the slope, if the respective conditions are fulfilled. A corollary to this conjecture is that in the limit of time n and chainlength L to infinity, the Frobenius-Perron equation of the respective class \mathcal{P} -dynamical systems always provides “nice”, i.e., the correct diffusive eigenmodes. As another corollary, it follows that there is no anomalous diffusion in class \mathcal{P} -maps, i.e., that normal diffusion is “typical” for such piecewise linear maps. A rigorous mathematical proof of Conjecture 2 seems to be possible along the lines of first passage and transition matrix method [104].

Results based on this method shall be presented in the next section. They have been verified by another numerical method [58,77,104], by another analytical method which has been implemented numerically [58,120], as well as, to a certain degree, by straightforward computer simulations [58,104]. Meanwhile, the same results have been obtained by J. Groeneveld with a different method [121], and they have also partly been reproduced by cycle expansion techniques [6].

IV. FRACTAL DIFFUSION COEFFICIENTS: RESULTS

Based on the methods presented in the previous section, the parameter-dependent diffusion coefficient $D(a)$ has been computed numerically for map \mathcal{L} for a broad range of values of the slope. The main results are shown in Fig. 8. The numerical precision obtained depends on the convergence of the diffusion coefficient with the chainlength, cf. Eq.(32), and is better than 10^{-4} for each $D(a)$ so that error bars do not appear in the diagrams. It should be emphasized that the numerical method employed here was the first one by which these curves of $D(a)$ have been obtained. It is by far not the most efficient one of the procedures developed up to now to compute deterministic diffusion coefficients [58,77,104,120,121]. However, it turns out to be very useful as well to compute other deterministic transport coefficients, e.g., chemical reaction rates [38], where more efficient methods fail.

Fig. 8 (a) shows the diffusion coefficient of map \mathcal{L} for values of the slope in the range $2 \leq a \leq 8$. The strength of diffusion clearly increases globally by increasing the slope from $a = 2$ to $a = 8$. This might be expected intuitively, since the probability of a particle to escape out of a box, as well as the mean distance a particle travels by performing a jump, are getting larger by increasing the value of the slope [58,78]. However, the increase of the diffusion coefficient is not monotonic and consists of oscillations not only at integer values of the slope, as has already been mentioned in Section II, but also on much finer scales between integer values. In fact, Fig. 8 (a) shows a certain regularity in the appearance of “wiggles”, i.e., local maxima and minima. If one denotes the local maxima at odd integer slopes a as wiggles of 0th order and any smaller local maxima systematically as wiggles of higher order, one can find one maximum of first order below $a = 3$, three maxima of first order in the range $3 \leq a \leq 5$, five maxima of first order in the range $5 \leq a \leq 7$, ... This regularity even persists to a certain extent on finer scales, although according to a slightly different rule, as can be seen, e.g., in the magnification Fig. 8 (f), $6 \leq a \leq 7$, where exactly six wiggles of second order appear between the respective wiggles of first order. In the same way, six wiggles of third order can be

observed in this region in further magnifications, and similar structures show up in the region of $4 \leq a \leq 5$ with four wiggles of second and four wiggles of third order. The region of $2 \leq a \leq 3$ is somewhat special and will be discussed separately. Thus, while the number of wiggles of first order increases by a step of two with increasing the slope, the number of wiggles of higher order remains constant in the region between two respective wiggles of first order, even by increasing the order of the wiggles to be considered. On the other hand, magnifications of other regions of the slope show that the structure of the curve is not everywhere that simple. For example, blow-ups of the regions $3 \leq a \leq 4$, Fig. 8 (b), and $5 \leq a \leq 6$, Fig. 8 (d), do not enable a clear distinction between “wiggles of different orders” anymore. Instead, they provide more complex structures which further magnifications, as, e.g., Figs. 8 (c) and (e), reveal to be self-similar.

It can be summarized at this stage that different regions of the curve exhibit different kinds of self-similarity, partly being fairly simple, but partly also being highly non-trivial. Thus, the results of Fig. 8 suggest that the parameter-dependent diffusion coefficient $D(a)$ for map \mathcal{L} is fractal [122]. More evidence for the fractality of the curve can be obtained in three different ways: Firstly, qualitative and quantitative explanations for the wiggles in certain regions of the slope will be provided, which ensure that these regions exhibit non-trivial self-similar behavior. This will be demonstrated in the following. Secondly, it is striking to observe that especially diagrams (c), (e), and (f) resemble graphs of some fractal functions, which have been obtained in Refs. [33,34,123] by working on dynamical systems being very similar to the ones considered here. These functions have been shown to possess fractal dimensions close to one [123]. On the one hand, this gives further evidence for the fractality of the curves of Fig. 8. On the other hand, this raises the new question whether there is an analytical fractal representation for certain regions of the curve, or maybe even for the full parameter-dependent diffusion coefficient of map \mathcal{L} . This problem is discussed in detail in Refs. [58,120]. Thirdly, it should be mentioned that numerical computations of the box counting dimension (or capacity) [66] of the curve have been performed. The results indicate that the curves shown in Fig. 8 (a) - (f) have fractal dimensions d very close to, but not equal to one in a range of $d = 1 + \Delta d$, $0 < \Delta d \leq 10^{-2}$. Because of the limited data set better values are difficult to get, especially since the fractal dimension is expected to be close to one in this case. Nevertheless, more detailed investigations of the fractal dimension for various regions of the curve could be of much interest. With respect to the magnifications in Fig. 8, it may even be conjectured that the full $D(a)$ -curve has locally different values of fractal dimensions.

Fig. 9 illustrates the principles of a first qualitative approach to understand the occurrence of wiggles of 0th and 1st order. It will be called *plus-minus approach*. The basic idea of this approach is to establish a connection between the appearance of wiggles in the $D(a)$ -graphs and the occurrence of certain dynamical correlations in the chain of boxes. These correlations are a main feature of transport of particles from one box to another, and they show up and disappear by varying the slope of the map. In the following, particles will be referred to solely by their positions, i.e., by points on the real line. Fig. 9 (a) and (b) sketch correlations of 0th order: As a starting point, the escape of particles out of one box in one direction, i.e., to the right, will be considered for varying the slope in the range $2 \leq a \leq 4$. Such an escape of points is related to a certain subinterval of the box which will be called *escape region*, as is shown in the figure. If points get mapped to the right at the next iteration, the respective subinterval will be denoted with a plus sign. The same way, subintervals will be denoted with a minus if points get mapped to the left. Therefore, the escape region marked in Fig. 9 is part of a plus region, and for small enough slope after only one iteration points of it get mapped directly into another plus region. This enhances diffusion, since particles can move continuously in one direction, i.e., here to the right. The behavior persists for increasing the slope up to $a = 3$. For slopes above this value, an increasing number of points of the escape region is now mapped into the minus region of the next box. This way, one obtains a “plus-minus” correlation, which means that particles either get slowed down, or even get scattered back into the previous box at the next iteration, which is surely bad for obtaining a strong diffusion coefficient. This game can be played by gradually increasing the value of the slope and leads to the qualitative “curve” in Fig. 9 (b), which explains the oscillations at integer slopes and the wiggles of 0th order, respectively. The sequences which mark the extrema in this graph give the symbolic dynamics of orbits close to, but less than $x = 1/2$ after one iteration with respect to the reduced map Eq.(33), where the region $0 < x \leq 1/2$ has been labeled with a plus and $1/2 < x \leq 1$ with a minus.

In Fig. 9 (c) the number of iterations has been increased to two. The method is the same as explained before, however, a further distinction has been made after the first iteration: new subintervals have been defined, which refer to points of the escape region being mapped to another plus or minus region at the second iteration. One can see that increasing the slope corresponds to creating different plus-minus sequences for orbits close to, but less than $x = 1/2$. This leads to the particles being in a good or bad position for going further in one direction with respect to the next iteration, depending on the value of the slope. The $D(a)$ -graph in Fig. 9 (d) again gives the qualitative behavior of $D(a)$ to be expected with respect to the dynamical correlations after two iterations, up to $a = 5$. This result corresponds well to the number of wiggles of first order estimated in the respective regions of the slope. Again, the plus-minus sequences give the symbolic dynamics of points close to, but less than $x = 1/2$ after two iterations.

The plus-minus method works on this level as well for any higher values of the slope and leads to a qualitative

explanation of the number of wiggles of first order for any region of the slope. To a certain degree, it can even explain additional features of the structure of the $D(a)$ -curves: For example, in Fig. 8 (b) one observes that the local maximum is not precisely at $a = 3$, although this could be expected from the results of the plus-minus method of 0th order. Actually, particles of the escape region close to $x = 1/2$ can still reach a good position for further movement in one direction, even for slopes slightly above $a = 3$. This is due to the fact that, although such points get first scattered back into the previous box after two iterations, here they are now in an excellent position for further jumps to the right again. This way, these orbits perform a kind of “spiral” and seem to be responsible for the surprising fact that the odd integer slope values of $D(a)$ are *not* precisely identical to the local extrema of the curve, but that there is always a kind of overhang, i.e., a further increase of the diffusion coefficient right above odd integer slopes, as, e.g., is shown in detail in Fig. 8 (c).

Although the plus-minus method can be applied to achieve a qualitative understanding of the wiggles of 0th and 1st order, further refinements of this method to obtain wiggles of higher order generally turned out not to be very promising. The main reason is that in case of more iterations of points of the escape region, the dynamics is getting quite complicated and is not easy to handle anymore in the qualitative way illustrated in Fig. 9. However, the basic idea of this method can be made more quantitative by a procedure which shall be called *turnstile dynamics*. The principle of turnstile dynamics is again to investigate the appearance and disappearance of long-range dynamical correlations by iterating points with respect to varying the slope. The new feature is now that not the full intervals of all single boxes are taken into account. Instead, the analysis is restricted solely to the regions of the boxes where transport of particles from one box to another occurs in form of jumps. These regions are called *turnstile*s:

Definition 3 (turnstile) *Turnstiles are the “coupling regions” of the single boxes of a chain of class \mathcal{P} , where points of one unit interval get mapped outside that particular interval into another unit interval.*

This notation has been adapted from the theory of transport of two-dimensional twist maps, such as sawtooth maps, where turnstiles are crucial for understanding large-scale diffusion [124–127]. The escape region introduced above in the context of the plus-minus method represents precisely one half of such a turnstile. The main idea is to study the *interaction* of turnstiles, i.e., by varying the slope it shall be investigated whether one obtains “good” or “bad” conditions for particles to get from one turnstile into another, or maybe even to get mapped successively through a series of turnstiles. As before in case of the plus-minus method, such dynamical correlations are expected to show up in the curve for the parameter-dependent diffusion coefficient $D(a)$. The advantage of turnstile dynamics is that it can be made quantitative by exemplifying all turnstiles with certain points of these regions. For instance, the peak of the turnstile one starts with may be represented by the critical point, $x = 1/2$. Now, one can try to compute the slopes for which this point maps into other turnstiles again, being exemplified by certain points, after certain numbers of iterations.

This has been done in detail for the region $2 \leq a \leq 3$, as shown in Fig. 10. The dashed line in the figure represents the prediction of $D(a)$ for a simple random-walk model as suggested in Ref. [46], which is discussed in detail in Refs. [58,77,78]. Note that, on a large scale, the model correctly accounts for the behavior of $D(a)$ near $a = 2$, but that with respect to any fine structure, such a simple model is clearly totally apart. One can see three distinct series of values of a in the figure. To understand the nature of these series, one should consider the orbit of the critical point. The first iterate of $x = 1/2$ is in the second interval, $(1, 2)$. The *series α* values of a are defined by the condition that the second iterate of $x = 1/2$ is at the leftmost point of the upward turnstile in the second interval $(1, 2)$ ($a = 2.732$), or that the third iterate is at the corresponding point in the third interval ($a = 2.920$), etc. The numbers on the $D(a)$ -curve refer to the number of intervals the image of $x = 1/2$ has travelled before it gets to the appropriate point on the turnstiles. *Series β* points are defined in a similar way, but they are allowed to have two or more internal reflections within an interval before reaching the left edge of a turnstile. *Series γ* points are defined by the condition that some image of $x = 1/2$ has reached the rightmost edge of an upward turnstile, i.e., some point $x = k + 1/2$, where k is an integer. One observes that each series produces a cascade of apparently self-similar regions of decreasing size, as the limits $a \rightarrow 2$ or $a \rightarrow 3$ are approached. These cascades provide a basis for a physical understanding of the features of $D(a)$ in this region: Particles leave a particular unit interval through a turnstile and undergo a number of iterations before they are within another turnstile. Whether they continue to move in the same or in the reverse direction at the next and later turnstiles is a sensitive function of the slope of the map. Thus, the fractal structure of the $D(a)$ curve is due to the effects of long-range correlations among turnstiles, and these correlations lead to changes of $D(a)$ on an infinitely fine scale. We note that another way to understand this fractal structure is in terms of so-called “pruning” of the microscopic deterministic dynamics. That is, by varying the parameter a certain types of orbits may suddenly disappear. This means that with respect to a given symbolic dynamics of the map certain symbol sequences, which identify the orbits, do not exist anymore. This can be related to the irregularities of the diffusion coefficient [6,50].

One should note that series γ points completely label the maxima of higher order introduced before, and series β points mark the respective minima. This way, in the region of the slope $a \leq 3$ the picture of quantitative turnstile dynamics is in full agreement with the results obtained by the qualitative plus-minus method outlined above (the

agreement has been checked to persist at least up to a level of extrema of second order). However, the application of turnstile dynamics has its limits: First, this method is of no use anymore for any higher value of the slope above $a = 3$. Thus, there is no other understanding of the structure in this range than the one provided qualitatively by the plus-minus approach. And second, even for values below $a = 3$ turnstile dynamics is quantitatively not completely correct: Apart from the lack of explaining the existence of the overhang above $a = 3$, a detailed analysis reveals further “tiny overhangs” at maxima of higher order, as, e.g., right above the maximum of first order in the region $2 \leq a \leq 3$ at $a = 2.414$ [128]. In other words, the “turnstile values” marked in Fig. 10 by series γ -points represent not the exact local maxima of higher order of the curve. The true local maxima are in fact shifted slightly to the right from these points, as in case of $a = 3$. The phenomenon of overhangs are further elucidated in Ref. [58,120]. However, apart from the qualitative remarks in the context of the plus-minus approach and the additional insight provided by the approach in Ref. [58,120], a detailed explanation of these overhang effects is still missing.

Since turnstile dynamics points seem to separate self-similar regions, it is suggestive to use them as a tool to do some scaling. Series α -values are especially suitable for this purpose, because they form a series of points which converges monotonically to $a = 3$, defining self-similar regions of decreasing size. These regions have been scaled according to the size of the intervals of the slope and of the respective diffusion coefficient intervals defined by

$$\begin{aligned} \Delta a_i &:= a(\text{series } \alpha\text{-point } (i+1)) - a(\text{series } \alpha\text{-point } i) \\ \Delta D_i &:= D(\text{series } \alpha\text{-point } (i+1)) - D(\text{series } \alpha\text{-point } i) \quad , \quad i = 0, \dots, 4 \end{aligned} \quad (40)$$

(note that $a = 2$ has been taken here as series α point 0). To obtain scaling factors, the fractions

$$s_a(i) := \frac{\Delta a_{i-1}}{\Delta a_i} \quad \text{and} \quad s_D(i) := \frac{\Delta D_{i-1}}{\Delta D_i} \quad (41)$$

have been computed. They led to the two series of values given in Table I. $s_a(i)$ seems to converge quite rapidly to a value around 3, whereas $s_D(i)$ approaches not that fast a value apparently between 2 and 3, but this is no more than a guess based on the first five values of two infinite series, since the data set of slopes and $D(a)$ -values is not sufficient for obtaining better results. At least these values suggest that some quantitative scaling is possible in this region.

At this point, it should be stressed that the region below $a = 3$ is special, compared to any other region of the slope: Firstly, the structure of the curve is remarkably simple, as shown in Fig. 10. Secondly, the number of wiggles of higher order is not constant with increasing order, but grows according to the structure described by the turnstile dynamics performed above. This is in contrast to the behavior of $D(a)$ in the ranges $4 \leq a \leq 5$ and $6 \leq a \leq 7$, where one may have expected similar generalities. Thirdly, the region below $a = 3$ is the only one which is simple enough such that turnstile dynamics can successfully be applied at all, and this region seems to provide some simple scaling laws. All this nice behavior suddenly breaks down at the value $a = 3$, which is marked by the largest overhang of the whole curve. Therefore, it might be assumed that the point at $a = 3$ separates regions of fundamental different dynamical behavior of the map, i.e., the dynamics seems to be sufficiently simple below, but suddenly gets quite complicated above this value. In fact, there is further evidence that such a transition exists, as is discussed in detail in Refs. [58,78].

Finally, another interesting feature of the parameter-dependent diffusion coefficient for map \mathcal{L} shall be pointed out. To obtain Fig. 11, the first “derivative” of the $D(a)$ -curve of Fig. 8 has been computed with respect to the full data set of $D(a)$ -values available. This has been done in linear approximation, i.e., two adjacent points of the data set have been connected with straight lines, and the “derivative” $D'(a) := \Delta D / \Delta a$ for $\Delta a \ll 1$ has been computed. However, since the curve of $D(a)$ is expected to be nowhere differentiable with respect to the slope, the derivative defined above should be better denoted as a “pseudo-derivative”, i.e., as a kind of mean value of ΔD over tiny regions of Δa which are approaching zero. Thus, the pseudo-derivative presented in Fig. 11 is mathematically not well-defined. Nevertheless, the numerical results turn out to be quite reasonable in the sense that they reflect to a certain degree the fractal structure of the actual $D(a)$ -curve. For instance, the three “bands” right above $a = 2$ seem to be due to the “triangle-like” self-similar structure of the region presented in Fig. 11, and the “bursts” at odd integer values correspond to the occurrence of local maxima and to the deformations of simple self-similar structures. We remark that in Fig. 11 the number of slopes for which $D(a)$ -values have been calculated is not homogeneously distributed over the whole range $2 \leq a \leq 8$, but that the number of points per interval is greater in certain regions of the slope, as, e.g., right above $a = 2$, $a = 3$ and around $a = 5.6$. These regions thus show up as slightly pronounced parts in the derivative plot, however, the structure of the curve does not seem to be affected by it. More details of this curve are discussed in Refs. [58,120].

V. SUMMARY

A. Conclusions

(1) A simple model for deterministic diffusion has been discussed where the microscopic scattering rules can be changed by varying a single control parameter. The diffusion coefficient of this model has been computed for a broad range of parameter values and shows a fractal structure as a function of the slope of the map. This result appears to be the first example of a dynamical system whose diffusion coefficient has an unambiguously fractal structure.

(2) A general method to compute parameter-dependent diffusion coefficients for a whole class of piecewise linear maps has been developed. It is based on the first passage method, which provides the definition of the diffusion coefficient for the dynamical system, in combination with the use of Markov partitions and transition matrices, which have been employed to solve the Frobenius-Perron equation of the dynamical system. For periodic boundary conditions, the parameter-dependent diffusion coefficient could be related to the second largest eigenvalue of the topological transition matrix. This method provides analytical solutions in simple cases and is also accessible to numerical implementations.

(3) The method described above has also been applied to absorbing boundary conditions. Long-range boundary layers have been found in the eigenmodes of the deterministic dynamical system. They also show up in quantitative calculations of the diffusion coefficient.

(4) Certain limits of the first passage method in combination with the use of transition matrices have been discussed: Drawbacks are especially the restriction to certain initial probability densities suitable for the application of transition matrices, as well as the “external” definition of the diffusion coefficient by the “matching eigenmodes” procedure of first passage. It turned out that this procedure is not well-defined anymore for smaller eigenmodes of the dynamical system.

(5) A systematical way to find Markov partitions for the class of maps under consideration has been developed. This method has been used as the basis for computing the parameter-dependent diffusion coefficient for the dynamical system mentioned above. For this map, as well as for the whole class of maps under consideration, Markov partitions are conjectured to be dense in the set of parameter values.

(6) A large number of eigenvalue problems of topological transition matrices, based on Markov partitions, has been solved numerically to compute the parameter-dependent diffusion coefficient for the model. In the course of these calculations, the reliability of well-known standard software routines for computing eigenvalue spectra has been checked critically, and numerical uncertainties have been pointed out.

(7) Certain large- and small-scale structures in the eigenmodes of the topological transition matrices have been found. The large-scale structures support the existence of statistical diffusion in the dynamical system, whereas the small-scale structures refer to the specific microscopic deterministic dynamics of the model system. These results suggest that the strength of the fractal diffusion coefficient is related to the fine-scale structure of the eigenmodes.

(8) A conjecture about the existence of diffusion coefficients for a broad class of one-dimensional maps has been made. This conjecture may shed more light on the origin of diffusion generated by a simple deterministic dynamical system and may show a way how to put the theory outlined in this article onto more solid mathematical grounds.

(9) Qualitative explanations for the structure of the parameter-dependent diffusion coefficient over the full range of parameter values have, to a certain extent, been provided by simple heuristic considerations.

(10) A more refined “turnstile dynamics” has been developed as a more quantitative approach to explain the structure of the parameter-dependent diffusion coefficient. It works in certain regions of the parameter values and provides a starting point for a scaling of certain self-similar structures.

(11) By employing these qualitative and quantitative methods, certain interesting features of the diffusion coefficient have been discussed, i.e., the phenomenon of “overhangs” at local extrema, and the special simple character of an “initial region” for small parameter values, where diffusion sets in.

(12) The numerically computed pseudo-derivative of the parameter-dependent diffusion coefficient seems to provide another characteristic property of fractal diffusion coefficients.

B. Outlook

The class of one-dimensional piecewise linear maps we have studied here by analyzing an example appears to be the most simple type of deterministic diffusive systems one can think of. Nevertheless, we have shown that the diffusion coefficient of such a map changes in a fractal way by varying a control parameter. Starting from this fundamental result, there are at least two directions in which our research can be pursued: One way is to study whether other transport quantities, like electric conductivities, chemical reaction rates, or magnetoresistances can exhibit such an irregular behavior as well. Another way is to investigate whether fractal transport coefficients exist in more complicated, and thus more realistic, dynamical systems.

First steps in these directions have already been taken: For example, a bias has been added to the simple map discussed in this paper. This generates an average current of particles which again exhibits fractal structures by varying the bias as a parameter [104,121]. Moreover, for small enough bias the current can run opposite to the bias [104,121], and for other parameter values the diffusion coefficient is zero with nonzero current [104]. Deterministic diffusion coefficients and deterministic currents which change irregularly by varying respective parameters have also been found in parameter-dependent two-dimensional multibaker models [38,39]. In their transport properties, these models are closely related to the class of one-dimensional maps discussed here. However, in addition they provide more physical features like being time-reversible [39,104] and being area-preserving or dissipative in a well-defined sense. Negative currents have been observed in these systems as well, and a parameter-dependent diffusive-reactive multibaker yields chemical reaction rates which are also fractal in a parameter [38].

In the periodic Lorentz gas, however, there is up to now no clear indication about a fractal behavior of transport coefficients. First results of computer simulations for the diffusion coefficient with respect to varying the density of scatterers show a very smooth curve, which indicates that if there are fractal fluctuations in the parameter at all they must occur on a very fine scale [129]. On the other hand, for the thermostated periodic Lorentz gas with an electric field computer simulations of several groups show clearly a very irregular behavior of the conductivity by varying the field strength [20,28,29,31]. In one case, the numerical results could even be confirmed by calculations based on cycle expansions [31].

Whether deterministic phenomena of this kind play a role in real statistical, experimentally accessible systems is a very open question. Following the chaotic hypothesis of Gallavotti and Cohen [130,131], one may believe that these phenomena are rather due to the simplicity of the models and should eventually disappear if the systems are getting more complex. Respectively, we would expect that certain necessary conditions must be fulfilled for systems to exhibit characteristics of fractal transport coefficients which may contradict the spirit of the chaotic hypothesis, such as being spatially periodic, low-dimensional, and such that particle-particle interactions are not of main importance. Physical systems of this kind could - to a certain extent - already be realized experimentally in form of so-called antidot lattices. Here, magnetoresistances which fluctuate irregularly by varying the field strength have already been observed experimentally in a classical limit [132,133], and to a certain extent they have been explained theoretically by identifying special orbits in the microscopic dynamics [134,135]. Another candidate of a system where certain irregularities in transport could be of a deterministic origin are so-called ratchets, where negative currents have already been found experimentally, as well as in theoretical models (see, e.g., Refs. [136,137] and further references therein). In fact, it can be argued that there exists a relation between certain types of ratchets and the class of one-dimensional maps (supplemented by a bias) studied here [104,138].

Fractal transport coefficients in one-dimensional maps actually appear to be stable with respect to imposing different kinds of random perturbations on the system [104]. This means that the fractal structure gradually smoothes out by increasing the perturbation strength and thus survives in form of irregular oscillations on finer scales if the perturbation is small enough. Although there are exceptions to this behavior [139], we believe this to be the typical scenario of how a possible fractality of parameter-dependent transport coefficients may appear if the system is not completely deterministic.

ACKNOWLEDGMENTS

This work is part of a Ph.D. thesis performed at the Technical University of Berlin [58]. R.K. and J.R.D. want to thank Chr. Beck, L. Bunimovich, P. Gaspard, C. Grebogi, B. Hunt, H.E. Nusse, R. Kapral, A. Pikovsky, and J. Yorke for helpful discussions. Special thanks go to J. Groeneveld for enlightening e-mail discussions and for critical comments on parts of this work. R.K. gratefully acknowledges financial support by the German Academic Exchange Service (DAAD), by the NaFöG commission Berlin, and by the Deutsche Forschungsgemeinschaft (DFG). He also wants to thank the Institute for Physical Science and Technology (IPST), College Park, and T.R. Kirkpatrick for their hospitality during a 1 1/2-year stay when this work got started, and for support in several subsequent visits. Finally, R.K. wants to thank S. Hess and E. Schöll for their interest in this work and for their continuous support.

APPENDIX A: TRANSITION MATRIX METHOD FOR CALCULATING DIFFUSION COEFFICIENTS

In this Appendix, we deal with the problem of how to solve analytically the eigenvalue problems of the topological transition matrices $T(a)$ formally introduced in Section III A. These transition matrices are the key ingredients of the Frobenius-Perron matrix equation, Eq. (13), and their eigenmodes and eigenvalues determine the deterministic

diffusive dynamics of the map at the respective parameter value of the slope, as outlined in Section II. Two simple examples of such transition matrices have already been given by Eq. (14) and Eq. (24), the problem of transition matrices for more complicated Markov partitions has been discussed in Section III B.

In the first subsection of this Appendix, we will consider integer slopes with periodic boundary conditions. In this case, trivial Markov partitions can be found for which the corresponding transition matrices have a simple structure. We analytically solve the eigenvalue problems of these transition matrices by standard methods and compute the parameter-dependent diffusion coefficients as defined by the first passage method. In the second subsection, we solve the eigenvalue problems of the respective transition matrices for two integer slopes with absorbing boundary conditions, namely for $a = 3$ and $a = 4$. In the third subsection, we discuss the problem of non-trivial Markov partitions for non-integer slopes. We depict Markov partitions for some special values of the slope, sketch the corresponding transition matrices, outline how to solve their eigenvalue problems analytically, and give the results for their eigenvalues and diffusion coefficients.

1. Integer slopes with periodic boundary conditions

As discussed in Section III, for periodic boundary conditions all topological transition matrices corresponding to Markov partitions are block circulants. For certain values of the slope it is possible to reduce these block circulants to simple circulants for which it is known how to solve their eigenvalue problems [100–102]. We employ here the approach of Berlin and Kac as described in App. A of Ref. 5 [100]. We summarize their main formulas and use them first to solve the problem of even integer slopes for periodic boundary conditions. We then treat analogously the slightly more complicated case of odd integer slopes.

Let T be a cyclic matrix of the type

$$T := \begin{pmatrix} t_1 & t_2 & t_3 & \cdots & t_{L-1} & t_L \\ t_L & t_1 & t_2 & \cdots & t_{L-2} & t_{L-1} \\ t_{L-1} & t_L & t_1 & \cdots & t_{L-3} & t_{L-2} \\ \vdots & & \vdots & & \vdots & \vdots \\ t_2 & t_3 & t_4 & \cdots & t_L & t_1 \end{pmatrix} . \quad (\text{A1})$$

We want to calculate the eigenvalues χ_m and the eigenvectors $|\phi_m\rangle$ associated with T , that is,

$$T|\phi_m\rangle = \chi_m|\phi_m\rangle \quad , \quad m = 0, \dots, L-1 \quad . \quad (\text{A2})$$

According to Ref. [100], the eigenvalues are given by

$$\chi_m = \sum_{s=1}^L t_s r_m^{s-1} \quad (\text{A3})$$

with

$$r_m = \exp\left(i\frac{2\pi m}{L}\right) \quad , \quad (\text{A4})$$

and the corresponding eigenvectors are

$$\begin{aligned} |\phi_m\rangle &= (\phi_m^1, \phi_m^2, \dots, \phi_m^k, \dots, \phi_m^L)^* \quad , \quad \phi_m^k = \tilde{a}_m \phi_{m,1}^k + \tilde{b}_m \phi_{m,2}^k \quad , \\ \phi_{m,1}^k &:= \cos(\theta_m(k-1)) \quad , \quad \phi_{m,2}^k := \sin(\theta_m(k-1)) \quad , \\ k &= 1, \dots, L \quad , \quad \theta_m := \frac{2\pi m}{L} \end{aligned} \quad (\text{A5})$$

with \tilde{a}_m and \tilde{b}_m to be fixed by suitable normalization conditions.

We now compute the diffusion coefficient for all even integer slopes $a = 2k$, $k \in \mathbb{N}$, of map \mathcal{L} by solving the eigenvalue problem of the respective general transition matrix $T(a)$ of the system. This transition matrix can be constructed as discussed in Section III A by using the same Markov partition for all slopes, that is, the one which is depicted in Fig. 3. We find that the matrix corresponding to this Markov partition is a simple circulant with matrix elements of

$$t_1 = 2, t_2 = 1, \dots, t_{a/2} = 1, t_{a/2+1} = 0, \dots, t_{L-a/2+1} = 0, t_{L-a/2+2} = 1, \dots, t_L = 1 \quad . \quad (\text{A6})$$

The $(s + a/2 - 1)$ th row, $1 \leq s \leq L - a/2$, of the corresponding eigenvalue problem defined by Eq. (A2) is thus determined by

$$\phi_m^s + \dots + \phi_m^{s+a/2-2} + 2\phi_m^{s+a/2-1} + \phi_m^{s+a/2} + \dots + \phi_m^{s+a-2} = \chi_m \phi_m^{s+a/2-1} \quad . \quad (\text{A7})$$

According to Eq. (A3), the eigenvalues are

$$\chi_m = 2 + r_m + \dots + r_m^{(a-2)/2} + r_m^{L-(a-2)/2} + \dots + r_m^{L-1} \quad , \quad (\text{A8})$$

and by using Eq. (A4) we obtain explicitly

$$\chi_m = 2 + 2 \sum_{s=1}^{(a-2)/2} \cos(\theta_m s) \simeq a - \theta_m^2 \frac{a(a-1)(a-2)}{24} \quad (L \rightarrow \infty) \quad . \quad (\text{A9})$$

The corresponding eigenvectors are given by Eq. (A5). Note that the largest eigenvalue χ_0 is equal to the slope of the map. This is a consequence of the fact that the topological transition matrices discussed here can be mapped onto stochastic transition matrices and that the Perron-Frobenius theorem for non-negative matrices applies [32,140]. It can be proven that this property holds for any topological transition matrix of map \mathcal{L} which is defined on the basis of Markov partitions with periodic boundary conditions [104]. According to the matrix Frobenius-Perron equation, Eq. (13), the corresponding largest eigenmode determines the equilibrium state of the system, which is here simply uniform. In analogy to Eq. (21), the second largest eigenvalue gives the decay rate, and the respective second largest eigenmode governs the diffusive transport in the map. For slope $a = 2k$ we thus obtain a decay rate of

$$\gamma_{dec}(a) = \ln \frac{a}{\chi_1(a)} \simeq \frac{4\pi^2}{L^2} \frac{(a-1)(a-2)}{24} \quad (L \rightarrow \infty) \quad . \quad (\text{A10})$$

With Eq. (9), this gives a diffusion coefficient of

$$D(a) = \frac{L^2}{4\pi^2} \gamma_{dec}(a) = \frac{(a-1)(a-2)}{24} \quad . \quad (\text{A11})$$

We now want to do the same calculation for all odd integer slopes $a = 2k - 1$, $k \in N$, again by employing periodic boundary conditions. As a Markov partition for all these slopes we use the same partitioning underlying the transition matrix as given by Eq. (24), that is, its parts are all of length $1/2$. Here, the corresponding a -dependent transition matrix is a block circulant where the single blocks consist of 2×2 -matrices. To illustrate the general structure of this matrix, we give the first rows and columns of the special case $a = 5$ which is

$$T(5) = \begin{pmatrix} 1 & 1 & 0 & 1 & 0 & 0 & 0 & 0 & 0 & 0 & \dots \\ 1 & 1 & 0 & 1 & 0 & 1 & 0 & 0 & 0 & 0 & \dots \\ 1 & 0 & 1 & 1 & 0 & 1 & 0 & 0 & 0 & 0 & \dots \\ 1 & 0 & 1 & 1 & 0 & 1 & 0 & 1 & 0 & 0 & \dots \\ 1 & 0 & 1 & 0 & 1 & 1 & 0 & 1 & 0 & 0 & \dots \\ 0 & 0 & 1 & 0 & 1 & 1 & 0 & 1 & 0 & 1 & \dots \\ 0 & 0 & 1 & 0 & 1 & 0 & 1 & 1 & 0 & 1 & \dots \\ \vdots & & \vdots & & \vdots & & \vdots & & \vdots & & \dots \end{pmatrix} \quad . \quad (\text{A12})$$

We now write down the eigenvalue equation, Eq. (A2), for this matrix. By using the notation u_m^k for the k th odd component of $|\phi_m\rangle$ and v_m^k for the k th even component we obtain for k odd, $1 \leq k \leq L - 3$, $0 \leq m \leq L - 1$,

$$\begin{aligned} u_m^k + u_m^{k+1} + v_m^{k+1} + v_m^{k+2} + v_m^{k+3} &= \chi_m v_m^{k+1} \\ u_m^k + u_m^{k+1} + u_m^{k+2} + v_m^{k+2} + v_m^{k+3} &= \chi_m u_m^{k+2} \quad , \end{aligned} \quad (\text{A13})$$

supplemented by periodic boundary conditions for the respective first and last rows of the matrix. This leads to $v_m^k = u_m^{k+1}$, yielding an equation for u_m^k which reads

$$u_m^k + u_m^{k+1} + u_m^{k+2} + u_m^{k+3} + u_m^{k+4} = \chi_m u_m^{k+2} \quad , \quad (\text{A14})$$

again by providing respective periodic boundary conditions. Thus, we have reduced the eigenvalue problem for the initial block circulant of Eq. (A12) to the eigenvalue problem of a simple circulant as given by Eq. (A14). The same reduction procedure can be carried out for general odd integer value of the slope. The reduced eigenvalue equation then reads

$$u_m^k + \dots + u_m^{k+a-1} = \chi_m u_m^{k+(a-1)/2} \quad , \quad (\text{A15})$$

supplemented by respective periodic boundary conditions. With the Berlin-Kac method we obtain for the eigenvalues

$$\chi_m = 1 + 2 \sum_{s=1}^{(a-1)/2} \cos(\theta_m s) \simeq a - \frac{4\pi^2 m^2}{L^2} \frac{a(a^2-1)}{24} \quad (L \rightarrow \infty) \quad , \quad 0 \leq m \leq L-1 \quad . \quad (\text{A16})$$

The eigenvectors are given here by

$$\begin{aligned} |\phi_m \rangle &= (u_m^1, v_m^1, \dots, u_m^k, v_m^k, \dots, u_m^L, v_m^L)^* \quad , \quad u_m^k = \tilde{a}_m u_{m,1}^k + \tilde{b}_m u_{m,2}^k \quad , \quad v_m^k = u_m^{k+1} \quad , \\ u_{m,1}^k &:= \cos(\theta_m(k-1)) \quad , \quad u_{m,2}^k := \sin(\theta_m(k-1)) \quad , \\ k &= 1, \dots, L \quad , \quad \theta_m := \frac{2\pi}{L} m \end{aligned} \quad (\text{A17})$$

with \tilde{a}_m and \tilde{b}_m to be fixed by suitable normalization conditions. For the decay rate we get

$$\gamma_{dec}(a) \simeq \frac{4\pi^2}{L^2} \frac{(a^2-1)}{24} \quad (L \rightarrow \infty) \quad , \quad (\text{A18})$$

which leads to a diffusion coefficient of

$$D(a) = \frac{a^2-1}{24} \quad . \quad (\text{A19})$$

2. Integer slopes with absorbing boundary conditions

For absorbing boundary conditions, the corresponding transition matrices are no block circulants anymore, but they belong to the broader class of banded square block Toeplitz matrices, as pointed out in Section III A. For these matrices no general methods are known for solving their eigenvalue problems analytically. However, in certain cases analytical solutions can still be obtained by straightforward calculations, as we will show for the two integer values of slope $a = 3$ and $a = 4$.

We first consider the case $a = 4$. The transition matrix for this parameter value is identical to the one given by Eq. (14) except that the upper right and the lower left corners are filled with zeroes because of absorbing boundaries. The eigenvalue problem of this matrix can now be solved in analogy to the calculations performed by Gaspard in Ref. [32]. The eigenvalue equation, Eq. (A2), reads here

$$\phi_m^k + 2\phi_m^{k+1} + \phi_m^{k+2} = \chi_m \phi_m^{k+1} \quad , \quad 0 \leq k \leq L-1 \quad , \quad (\text{A20})$$

supplemented by the absorbing boundary conditions $\phi_m^0 = \phi_m^{L+1} = 0$. Since this equation is of the form of a discretized ordinary differential equation of degree two we make the ansatz

$$\phi_m^k = a \cos(k\theta) + b \sin(k\theta) \quad , \quad 0 \leq k \leq L+1 \quad . \quad (\text{A21})$$

The two boundary conditions then lead to

$$a = 0 \quad \text{and} \quad \sin((L+1)\theta) = 0 \quad (\text{A22})$$

yielding

$$\theta_m = \frac{m\pi}{L+1} \quad , \quad 1 \leq m \leq L \quad . \quad (\text{A23})$$

The eigenvectors are then determined by

$$\phi_m^k = b \sin(k\theta_m) \quad (\text{A24})$$

with b as the normalization constant. Putting this equation into Eq. (A20) gives as the eigenvalues

$$\chi_m = 2 + 2 \cos \theta_m \quad . \quad (\text{A25})$$

Note that in case of absorbing boundary conditions the largest eigenvalue is not equal to the slope of the map, but determines the escape rate of the system. Correspondingly, the largest eigenmode is the diffusive mode of the map. However, for $L \rightarrow \infty$ the largest eigenvalue goes to the exact value of the slope, which therefore serves as an upper limit of the eigenvalue spectrum. This is conjectured to be true for any topological transition matrix of map \mathcal{L} which is defined on the basis of Markov partitions by employing absorbing boundary conditions [104]. In the limit of chainlength $L \rightarrow \infty$ these results lead to the escape rate and diffusion coefficient presented in Section III A, Eqs. (30 – 32).

We now treat analogously the case of slope $a = 3$ for absorbing boundary conditions. We know from the previous subsection that for odd integer slopes the Markov partitions, and thus the respective transition matrices, are a bit more complicated. The transition matrix for $a = 3$ is identical to the one given by Eq. (24) except that the upper right and lower left corners are filled with zeroes because of absorbing boundaries, as before.

To write down the eigenvalue equation, Eq. (A2), for this matrix we use the same notation as in the previous subsection for odd integer slopes. With u_m^k being the k th odd component of $|\phi_m\rangle$ and v_m^k being the k th even component we obtain for k odd, $0 \leq k \leq L$,

$$\begin{aligned} u_m^k + v_m^k + v_m^{k+1} &= \chi_m v_m^k \\ u_m^k + u_m^{k+1} + v_m^{k+1} &= \chi_m u_m^{k+1} \quad , \end{aligned} \quad (\text{A26})$$

supplemented by the absorbing boundary conditions $u_m^0 = v_m^{L+1} = 0$. This again leads to $v_m^k = u_m^{k+1}$, yielding an equation for u_m^k which reads

$$u_m^k + u_m^{k+1} + u_m^{k+2} = \chi_m u_m^{k+1} \quad , \quad 0 \leq k \leq L \quad , \quad (\text{A27})$$

with the respective absorbing boundary conditions. We again use Eq. (A21) as an ansatz to solve this equation. The two boundary conditions then lead to

$$a = 0 \quad \text{and} \quad \sin((L+2)\theta) = 0 \quad (\text{A28})$$

yielding

$$\theta_m = \frac{m\pi}{L+2} \quad , \quad 1 \leq m \leq L+1 \quad . \quad (\text{A29})$$

The eigenvectors are then determined by

$$\begin{aligned} u_m^k &= b \sin(k\theta_m) \\ v_m^k &= b \sin((k+1)\theta_m) \end{aligned} \quad (\text{A30})$$

with b as the normalization constant. Putting this equation into Eq. (A27) gives as eigenvalues

$$\chi_m = 1 + 2 \cos \theta_m \quad . \quad (\text{A31})$$

In the limit of chainlength $L \rightarrow \infty$ this leads to the results for escape rate and diffusion coefficient presented in Section III A, Eqs. (30 – 32).

We remark that we do not have analytical solutions of the eigenvalue problems for integer values of the slope above $a = 4$ with absorbing boundary conditions. Here, the ansatz of Eq. (A21) does not seem to be sufficient because of long-range boundary layers which are induced by the absorbing boundary conditions, see also the remarks in Section III A to this problem.

3. Non-trivial Markov partitions with periodic boundary conditions

In this subsection, we discuss some examples of non-trivial Markov partitions where analytical solutions of the respective eigenvalue problems of the transition matrices can still be obtained analytically. This can be done by

reducing block circulants onto simple circulants in the way illustrated in the previous subsections for odd integer slopes. In the following, we will only consider periodic boundary conditions, because then the general method of Berlin and Kac to solve the respective eigenvalue problems can be applied.

We discuss two different series of Markov partitions. For the simplest case of the first series we briefly outline of how to perform the calculations, and we give the results for the eigenvalues and the diffusion coefficient. For the next parameter value of this series we give only the main results, before writing down the respective general formulas for the whole series. For the second series we only deal with the first two parameter values by giving the main results.

In each case we proceed by first depicting a box map of the full chain of boxes with its Markov partition in a figure. We indicate of how the respective Markov partition has been computed and give the exact value of the slope by which it is defined. On this basis, we sketch the corresponding transition matrix for the full chain of boxes and give the main results for eigenvalues and diffusion coefficient.

a. Series 1

As has been pointed out in Section III B, a Markov partition is defined via a generating orbit which obeys Eq. (36). By using the notation of this equation, the first series of Markov partitions discussed here is characterized by $\delta = 0$ and the number of iterations of the reduced map being $n = 1$. The first case of this series is obtained from the solution of this equation for the slope a being restricted between 2 and 4. The second case refers to $4 < a < 6$, the general case is for solutions $2k < a < 2(k + 1)$, $k \in \mathbb{N}$.

Case 1:

This is the simplest case and corresponds to the smallest slope of this series, as illustrated in Fig. 12 (a). As one can infer from the figure, the precise value of the slope can be computed from the equation

$$1 = 2(1 + \epsilon)\epsilon \quad 0 \leq \epsilon \leq 1/2 \quad , \quad (\text{A32})$$

where $a = 2(1 + \epsilon)$, which leads to the solution

$$a = (\sqrt{3} - 1)/2 \simeq 2.73205 \quad . \quad (\text{A33})$$

The partition of the full chain of boxes can be constructed by continuing the box map of Fig. 12 (a) periodically. The corresponding transition matrix can then be obtained from this partition as described in Section III B and reads

$$T(2.73205) = \begin{pmatrix} 1 & 0 & 1 & 0 & 0 & 0 & 0 & 0 & 0 & 0 & \cdots \\ 1 & 0 & 1 & 0 & 0 & 0 & 0 & 0 & 0 & 0 & \cdots \\ 1 & 0 & 1 & 0 & 1 & 0 & 0 & 0 & 0 & 0 & \cdots \\ 0 & 1 & 0 & 1 & 0 & 1 & 0 & 0 & 0 & 0 & \cdots \\ 0 & 0 & 0 & 1 & 0 & 1 & 0 & 0 & 0 & 0 & \cdots \\ 0 & 0 & 0 & 1 & 0 & 1 & 0 & 1 & 0 & 0 & \cdots \\ 0 & 0 & 0 & 0 & 1 & 0 & 1 & 0 & 1 & 0 & \cdots \\ \vdots & & & \vdots & & \vdots & & \vdots & & \vdots & \cdots \end{pmatrix} , \quad (\text{A34})$$

where the first, second, third, ..., three rows correspond to the first, second, third, ..., box of the chain. We now reduce this block circulant to a simple circulant. Since the Markov partition of each box consists of three parts, we use three different symbols u_m^k , v_m^k , w_m^k as components of the eigenvectors to write down the eigenvalue equation, Eq. (A2), of this matrix,

$$\begin{aligned} u_m^k + w_m^k &= \chi_m v_m^k \\ u_m^k + w_m^k + v_m^{k+1} &= \chi_m w_m^k \\ v_m^k + u_m^{k+1} + w_m^{k+1} &= \chi_m u_m^{k+1} \quad , \quad 1 < k < L \quad , \end{aligned} \quad (\text{A35})$$

supplemented by respective periodic boundary conditions for the first and the last row of the matrix. From these equations it is immediately obtained that

$$\begin{aligned} w_m^k &= \frac{v_m^{k+1} + \chi_m v_m^k}{\chi_m} \quad , \\ u_m^{k+1} &= \frac{v_m^k + \chi_m v_m^{k+1}}{\chi_m} \end{aligned} \quad (\text{A36})$$

which leads to

$$v_m^{k+1} + 2v_m^k + v_m^{k-1} = \chi_m^2 v_m^k \quad (\text{A37})$$

with respective periodic boundary conditions. This again defines the eigenvalue problem of a simple circulant which we can solve by the methods used before. For the eigenvalues we obtain

$$\chi_m = 1 \pm \sqrt{1 + 2 \cos \theta_m} \simeq 1 \pm \sqrt{3} \left(1 - \frac{\theta_m^2}{6}\right) \quad (L \rightarrow \infty) \quad , \quad \theta_m = \frac{2\pi m}{L} \quad , \quad 0 \leq m \leq L-1 \quad , \quad (\text{A38})$$

where the second largest eigenvalue yields a diffusion coefficient of

$$D(2.73205) = \frac{\sqrt{3}}{6(1 + \sqrt{3})} \simeq 0.10566 \quad . \quad (\text{A39})$$

As pointed out above, the largest eigenvalue is again identical to the slope of the map. It is related to an equilibrium eigenmode which is here a periodically continued piecewise constant function, based on the single parts of the Markov partition.

Case 2:

The second case of this series is the Markov partition defined by the respective value of the slope between 4 and 6. Its box map partition is illustrated in Fig. 12 (b) and corresponds to $a = 2 + \sqrt{8} \simeq 4.82843$. The transition matrix reads

$$T(4.8284) = \begin{pmatrix} 1 & 0 & 1 & 0 & 0 & 1 & 0 & 0 & 0 & 0 & \dots \\ 1 & 0 & 1 & 0 & 0 & 1 & 0 & 0 & 0 & 0 & \dots \\ 1 & 0 & 1 & 0 & 0 & 1 & 0 & 1 & 0 & 0 & \dots \\ 1 & 0 & 0 & 1 & 0 & 1 & 0 & 0 & 1 & 0 & \dots \\ 1 & 0 & 0 & 1 & 0 & 1 & 0 & 0 & 1 & 0 & \dots \\ 1 & 0 & 0 & 1 & 0 & 1 & 0 & 0 & 1 & 0 & \dots \\ 0 & 1 & 0 & 1 & 0 & 0 & 1 & 0 & 1 & 0 & \dots \\ 0 & 0 & 0 & 1 & 0 & 0 & 1 & 0 & 1 & 0 & \dots \\ 0 & 0 & 0 & 1 & 0 & 0 & 1 & 0 & 1 & 0 & \dots \\ 0 & 0 & 0 & 0 & 1 & 0 & 1 & 0 & 0 & 1 & \dots \\ \vdots & & \vdots & & \vdots & & \vdots & & \vdots & & \ddots \end{pmatrix} . \quad (\text{A40})$$

Again, this block circulant can be reduced to a simple circulant. By some calculations which are quite analogous to the ones of the previous example we obtain as eigenvalues

$$\chi_m = 1 + \cos \theta_m \pm \sqrt{(1 + \cos \theta_m)^2 + 2 \cos(2\theta_m) + 2 \cos(3\theta_m)} \simeq 2 - \frac{\theta_m^2}{2} \pm \sqrt{8} \left(1 - \frac{15}{16} \theta_m^2\right) \quad (L \rightarrow \infty) \quad , \quad (\text{A41})$$

θ_m and m as before, with a diffusion coefficient of

$$D(4.8284) = \frac{1 + \frac{15}{4} \sqrt{2}}{4(1 + \sqrt{2})} \simeq 0.65273 \quad . \quad (\text{A42})$$

General case of this series:

We now give the general solution for eigenvalues and diffusion coefficient of all cases of this series of Markov partitions. Let

$$a(p) = 2(p + 1 + \epsilon) \quad \text{with} \quad \epsilon = \frac{1}{2}(-p - 1 + \sqrt{2p + 2 + (p + 1)^2}) \quad , \quad p \in \mathbb{N}_0 \quad , \quad (\text{A43})$$

be the slope of map \mathcal{L} . Then $a(0)$ is the value of the slope of case 1 and $a(1)$ is the value of the slope of case 2. Any higher value of $a(p)$, $p > 1$, defines a Markov partition which is of the same type as in the two previous examples, that is, it fulfills the general definition of this series given at the beginning. For this series of Markov partitions the general eigenvalue problem of the corresponding transition matrices can be solved by generalizing the calculations above. This yields for the eigenvalues

$$\chi_m = 1 + \sum_{k=1}^p \cos(k\theta_m) \pm \sqrt{\left[\left(1 + \sum_{k=1}^p \cos(k\theta_m)\right)^2 + 2 \sum_{k=1}^{p+1} \cos((p+k)\theta_m) \right]} \quad , \quad 0 \leq m \leq L-1 \quad . \quad (\text{A44})$$

In the limit of $L \rightarrow \infty$, this leads to a diffusion coefficient of

$$D(p) = \frac{(2p^2 + p)\sqrt{(1+p)(3+p)} + 2p^3 + 17p^2 + 20p + 6}{12(\sqrt{(1+p)(3+p)} + 3 + p)} \quad . \quad (\text{A45})$$

b. Series 2

By again referring to Eq. (36), and using the notation of Section III B, a second series of Markov partitions is defined by $\delta = 1 - \epsilon$ and the number of iterations of the reduced map being $n = 1$. In the following we give the main results for only the first two cases of this series, which are based on the solution of this equation for the slope a being $2 < a < 4$, and $4 < a < 6$, respectively.

Case 1:

The partition illustrated in Fig. 12 (c) corresponds to the slope

$$a = \frac{1 + \sqrt{17}}{2} \simeq 2.56155 \quad (\text{A46})$$

and defines, periodically continued, a transition matrix of

$$T(2.56155) = \begin{pmatrix} 1 & 1 & 0 & 0 & 0 & 0 & 0 & 0 & 0 & 0 & \dots \\ 1 & 0 & 1 & 0 & 0 & 0 & 0 & 0 & 0 & 0 & \dots \\ 0 & 1 & 1 & 0 & 1 & 0 & 0 & 0 & 0 & 0 & \dots \\ 0 & 1 & 0 & 1 & 1 & 0 & 0 & 0 & 0 & 0 & \dots \\ 0 & 0 & 0 & 1 & 0 & 1 & 0 & 0 & 0 & 0 & \dots \\ 0 & 0 & 0 & 0 & 1 & 1 & 0 & 1 & 0 & 0 & \dots \\ 0 & 0 & 0 & 0 & 1 & 0 & 1 & 1 & 0 & 0 & \dots \\ 0 & 0 & 0 & 0 & 0 & 0 & 1 & 0 & 1 & 0 & \dots \\ 0 & 0 & 0 & 0 & 0 & 0 & 0 & 1 & 1 & 0 & \dots \\ 0 & 0 & 0 & 0 & 0 & 0 & 0 & 1 & 0 & 1 & \dots \\ \vdots & & & \vdots & & & \vdots & & & & \ddots \end{pmatrix} \quad . \quad (\text{A47})$$

The eigenvalues are

$$\chi_m = \frac{1}{2} \pm \sqrt{\frac{9}{4} + 2 \cos \theta_m} \quad , \quad \theta_m = \frac{2\pi m}{L} \quad , \quad 0 \leq m \leq L-1 \quad , \quad (\text{A48})$$

the diffusion coefficient is

$$D(2.56155) = \frac{2}{\sqrt{171} + \sqrt{17}} \simeq 0.09468 \quad . \quad (\text{A49})$$

Case 2:

The partition illustrated in Fig. 12 (d) corresponds to the slope

$$a = \frac{3 + \sqrt{41}}{2} \simeq 4.70156 \quad (\text{A50})$$

and defines, periodically continued, a transition matrix of

$$T(4.70156) = \begin{pmatrix} 1 & 0 & 1 & 0 & 1 & 0 & 0 & 0 & 0 & 0 & \cdots \\ 1 & 0 & 1 & 0 & 0 & 1 & 0 & 0 & 0 & 0 & \cdots \\ 1 & 0 & 1 & 0 & 0 & 1 & 0 & 1 & 0 & 0 & \cdots \\ 1 & 0 & 0 & 1 & 0 & 1 & 0 & 1 & 0 & 0 & \cdots \\ 1 & 0 & 0 & 1 & 0 & 1 & 0 & 0 & 1 & 0 & \cdots \\ 0 & 1 & 0 & 1 & 0 & 1 & 0 & 0 & 1 & 0 & \cdots \\ 0 & 1 & 0 & 1 & 0 & 0 & 1 & 0 & 1 & 0 & \cdots \\ 0 & 0 & 0 & 1 & 0 & 0 & 1 & 0 & 1 & 0 & \cdots \\ \vdots & & & \vdots & & & \vdots & & & & \ddots \end{pmatrix} . \quad (\text{A51})$$

The eigenvalues are

$$\chi_m = \frac{1 + 2 \cos \theta_m}{2} \pm \sqrt{\frac{1}{4}(1 + 2 \cos \theta_m)^2 + 2 + 2 \cos \theta_m + 2 \cos(2\theta_m) + 2 \cos(3\theta_m)} , \quad (\text{A52})$$

θ_m and m as before, the diffusion coefficient is

$$D(4.70156) = \frac{1 + \frac{31}{\sqrt{41}}}{3 + \sqrt{41}} \simeq 0.62122 . \quad (\text{A53})$$

We finally remark that analytical calculations which are similar to the ones performed here have been carried out in Refs. [6,50,51]. These calculations are based on cycle expansions, and the diffusion coefficient has been computed for different piecewise linear maps.

* Present address: Center for Nonlinear Phenomena and Complex Systems, Université Libre de Bruxelles, Campus Plaine, Code Postal 231, Boulevard du Triomphe, B-1050 Brussels, Belgium; e-mail: rklages@ulb.ac.be

- [1] D. Evans and G. Morriss, *Statistical Mechanics of Nonequilibrium Liquids*, (Academic Press, London, 1990).
- [2] W. G. Hoover, *Computational statistical mechanics* (Elsevier, Amsterdam, 1991).
- [3] A. Lichtenberg and M. Lieberman, *Regular and Chaotic Dynamics*, Vol. 38 of *Applied Mathematical Sciences*, 2nd ed. (Springer, New York, 1992).
- [4] *Microscopic simulations of complex hydrodynamic phenomena*, Vol. 292 of *NATO ASI Series B: Physics*, edited by M. Mareschal and B. L. Holian (Plenum Press, New York, 1992).
- [5] S. Wiggins, *Chaotic Transport in Dynamical Systems*, Vol. 2 of *Interdisciplinary Applied Mathematics* (Springer, New York, 1992).
- [6] P. Cvitanović, lecture notes, available on www.nbi.dk/ChaosBook/ (unpublished).
- [7] *The microscopic approach to complexity in non-equilibrium molecular simulations*, Vol. 240 of *Physica A*, edited by M. Mareschal (Elsevier, Amsterdam, 1997).
- [8] P. Gaspard, *Chaos, Scattering, and Statistical Mechanics* (Cambridge University Press, Cambridge, 1998).
- [9] J.R. Dorfman, lecture notes, Institute for Physical Science and Technology, College Park (to be published).
- [10] H. A. Posch and W. G. Hoover, *Phys. Lett. A* **123**, 227 (1987).
- [11] H. Posch and W. Hoover, *Phys. Rev. A* **38**, 473 (1988).
- [12] H. Posch and W. Hoover, *Phys. Rev. A* **39**, 2175 (1989).
- [13] D. Evans, E. Cohen, and G. Morris, *Phys. Rev. A* **42**, 5990 (1990).
- [14] C. Dellago, H. Posch, and W. Hoover, *Phys Rev E* **53**, 1485 (1996), 1063-651X.
- [15] H. van Beijeren and J. Dorfman, *Phys Rev Lett* **74**, 4412 (1995), 0031-9007.
- [16] M. Ernst, J. Dorfman, R. Nix, and D. Jacobs, *Phys Rev Lett* **74**, 4416 (1995), 0031-9007.
- [17] A. Latz, H. van Beijeren, and J. Dorfman, *Phys Rev Lett* **78**, 207 (1997), 0031-9007.
- [18] C. Dellago and H. Posch, *Phys Rev Lett* **78**, 211 (1997), 0031-9007.
- [19] J. Machta and R. Zwanzig, *Phys. Rev. Lett.* **50**, 1959 (1983).
- [20] B. Moran and W. Hoover, *J. Stat. Phys.* **48**, 709 (1987).
- [21] P. Gaspard and G. Nicolis, *Phys. Rev. Lett.* **65**, 1693 (1990).
- [22] P. Cvitanovic, P. Gaspard, and T. Schreiber, *Chaos* **2**, 85 (1992).
- [23] W. N. Vance, *Phys. Rev. Lett.* **69**, 1356 (1992).
- [24] N. Chernov, C. Eyink, J. Lebowitz, and Y. Sinai, *Phys. Rev. Lett.* **70**, 2209 (1993).

- [25] P. Gaspard, *Chaos* **3**, 427 (1993).
- [26] A. Baranyai, D. Evans, and E. Cohen, *J. Stat. Phys.* **70**, 1085 (1993).
- [27] P. Gaspard and F. Baras, *Phys. Rev. E* **51**, 5333 (1994).
- [28] J. Lloyd, M. Niemeyer, L. Rondoni, and G. Morriss, *Chaos* **5**, 536 (1995), 1054-1500.
- [29] C. Dellago, L. Glatz, and H. Posch, *Phys Rev E* **52**, 4817 (1995), 1063-651X.
- [30] P. Gaspard, *Phys Rev E* **53**, 4379 (1996), 1063-651X.
- [31] C. Dettmann and G. P. Morriss, *Phys. Rev. Lett.* **78**, 4201 (1997).
- [32] P. Gaspard, *J. Stat. Phys.* **68**, 673 (1992).
- [33] S. Tasaki and P. Gaspard, in *Towards the Harnessing of Chaos*, edited by M. Yamaguti (Elsevier, Amsterdam, 1994), pp. 273–288.
- [34] S. Tasaki and P. Gaspard, *J. Stat. Phys.* **81**, 935 (1995).
- [35] T. Tél, J. Vollmer, and W. Breymann, *Europhys Lett* **35**, 659 (1996), 0295-5075.
- [36] G. Morriss and L. Rondoni, *Physica A* **233**, 767 (1996), 0378-4371.
- [37] J. Vollmer, T. Tél, and W. Breymann, *Phys. Rev. Lett.* **79**, 2759 (1997).
- [38] P. Gaspard and R. Klages, *Chaos* **8**, 409 (1998)
- [39] R. Klages and T. Tél (unpublished)
- [40] S. Grossmann and H. Fujisaka, *Phys. Rev. A* **26**, 1179 (1982).
- [41] H. Fujisaka and S. Grossmann, *Z. Physik B* **48**, 261 (1982).
- [42] S. Grossmann and S. Thomae, *Phys. Lett. A* **97**, 263 (1983).
- [43] T. Geisel and J. Nierwetberg, *Phys. Rev. Lett.* **48**, 7 (1982).
- [44] T. Geisel and S. Thomae, *Phys. Rev. Lett.* **52**, 1936 (1984).
- [45] T. Geisel, J. Nierwetberg, and A. Zacherl, *Phys. Rev. Lett.* **54**, 616 (1985).
- [46] M. Schell, S. Fraser, and R. Kapral, *Phys. Rev. A* **26**, 504 (1982).
- [47] R. Artuso, *Phys. Lett. A* **160**, 528 (1991).
- [48] R. Artuso, G. Casati, and R. Lombardi, *Phys. Rev. Lett.* **71**, 62 (1993).
- [49] R. Artuso, *Physica D* **76**, 1 (1994).
- [50] H.-C. Tseng *et al.*, *Phys. Lett. A* **195**, 74 (1994).
- [51] C.-C. Chen, *Phys. Rev. E* **51**, 2815 (1995).
- [52] M. Dörfle, *J. Stat. Phys.* **93** (1985).
- [53] I. Claes and C. Van den Broeck, *J. Stat. Phys.* **70**, 1215 (1993).
- [54] R. Kluiwing, H. W. Capel, and R. A. Pasmarter, *Physica A* **164**, 593 (1990).
- [55] Y. Elskens and R. Kapral, *J. Stat. Phys.* **38**, 1027 (1985).
- [56] Z. Kaufmann, H. Lustfeld, A. Németh, and P. Szépfalussy, *Phys. Rev. Lett.* **78**, 4031 (1997).
- [57] P. Gaspard and F. Baras, in *Microscopic simulations of complex hydrodynamic phenomena*, Vol. 292 of *NATO ASI Series B: Physics*, edited by M. Mareschal and B. Holian (Plenum Press, New York, 1992), pp. 301–322.
- [58] R. Klages, *Deterministic diffusion in one-dimensional chaotic dynamical systems* (Wissenschaft & Technik-Verlag, Berlin, 1996).
- [59] R. Klages and J. Dorfman, *Phys. Rev. Lett.* **74**, 387 (1995).
- [60] N. Wax, *Selected Papers on Noise and Stochastic Processes* (Dover, New York, 1954).
- [61] G. Wannier, *Statistical Physics* (Dover, New York, 1966).
- [62] N. van Kampen, *Stochastic processes in physics and chemistry* (North Holland, Amsterdam, 1992).
- [63] F. Reif, *Statistische Physik und Theorie der Wärme*, 3rd ed. (de Gruyter, Berlin, 1987).
- [64] C. Beck and F. Schlögl, *Thermodynamics of Chaotic Systems*, Vol. 4 of *Cambridge nonlinear science series* (Cambridge University Press, Cambridge, 1993).
- [65] The term *piecewise linear* should be understood in the sense that the interval of the map which is periodically continued consists of a finite number of subintervals, on the interiors of which the map is linear.
- [66] E. Ott, *Chaos in Dynamical Systems* (Cambridge University Press, Cambridge, 1993).
- [67] M. Misiurewicz, *Dynamical Systems and Ergodic Theory*, Vol. 23 of *Banach Center Publications* (Polish Scientific Publishers, Warszawa, 1989), pp. 119–124.
- [68] L. Alsedà, J. Llibre, M. Misiurewicz, and C. Tresser, *Ann. Inst. Fourier, Grenoble* **39**, 929 (1989).
- [69] A. Katok and B. Hasselblatt, *Introduction to the Modern Theory of Dynamical Systems*, Vol. 54 of *Encyclopedia of Mathematics and its Applications* (Cambridge University Press, Cambridge, 1995).
- [70] J. Guckenheimer and P. Holmes, *Nonlinear Oscillations, Dynamical Systems, and Bifurcations of Vector Fields*, Vol. 42 of *Applied mathematical sciences*, 3rd ed. (Springer, Berlin, 1990).
- [71] H.-O. Peitgen, H. Jürgens, and D. Saupe, *Chaos and Fractals* (Springer-Verlag, Berlin, 1992).
- [72] P. Glendinning and C. Sparrow, *Physica D* **62**, 22 (1993).
- [73] J. Hubbard and S. C., *Comm. Pure Appl. Math.* **43**, 431 (1990).
- [74] L. Alsedà and J. Llibre, *Dynamical Systems and Ergodic Theory*, Vol. 23 of *Banach Center Publications* (Polish Scientific Publishers, Warszawa, 1989), pp. 83–89.
- [75] S. Grossmann and S. Thomae, *Phys. Lett. A* **97**, 263 (1983).

- [76] S. Thomae, in *Statics and Dynamics of nonlinear systems*, edited by C. B. at al. (Springer, Berlin, 1983), pp. 204–210.
- [77] R. Klages and J. Dorfman, *Phys Rev E* **55**, R1247 (1997), 1063-651X.
- [78] R. Klages and J. R. Dorfman (unpublished)
- [79] J. Dorfman and P. Gaspard, *Phys. Rev. E* **51**, 28 (1995).
- [80] P. Gaspard and J. Dorfman, *Phys. Rev. E* **52**, 3525 (1995).
- [81] A. Lasota and M. Mackey, *Chaos, Fractals, and Noise*, Vol. 97 of *Applied mathematical sciences*, 2nd ed. (Springer, Berlin, 1994).
- [82] J.-P. Eckmann and D. Ruelle, *Rev. Mod. Phys.* **57**, 617 (1985).
- [83] Y. Sinai, *Funktional'nyi analiz i Ego Prilozheniya* **2**, 64 (68).
- [84] Y. Sinai, *Funktional'nyi analiz i Ego Prilozheniya* **2**, 70 (1968).
- [85] R. Bowen, *Equilibrium states and the ergodic theory of Anosov diffeomorphisms*, Vol. 470 of *Lecture notes in mathematics* (Springer-Verlag, Berlin, 1975).
- [86] D. Ruelle, *Thermodynamic Formalism*, Vol. 5 of *Encyclopedia of mathematics and its applications* (Addison-Wesley, Reading, Mass., 1978).
- [87] R. Bowen, *Commun. Math. Phys.* **69**, 1 (1979).
- [88] I. Cornfeld, S. Fomin, and Y. Sinai, *Ergodic Theory* (Springer, New York, 1982).
- [89] Y. Sinai, *Dynamical Systems*, Vol. 2 of *Encyclopedia of mathematical sciences* (Springer, Berlin, 1989).
- [90] D. Ruelle, *Commun. Math. Phys.* **125**, 239 (1989).
- [91] J. Moore and S. Sengupta, *SIAM J. Control* **13**, 1103 (1975).
- [92] A. Boyarski and M. Scarowsky, *Trans. Am. Math. Soc.* **255**, 243 (1979).
- [93] N. Friedman and A. Boyarsky, *Lin. Alg. Appl.* **38**, 141 (1981).
- [94] W. Byers, P. Gora, and A. Boyarsky, *Ergod. Th. and Dynam. Sys.* **10**, 645 (1990).
- [95] Y. Elskens and R. Kapral, *J. Stat. Phys.* **38**, 1027 (1985).
- [96] P. Grassberger, *Z. Naturforsch.* **43a**, 671 (1988).
- [97] D. MacKernan and G. Nicolis, *Phys. Rev. E* **50**, 988 (1994).
- [98] N. Balmforth, E. Spiegel, and C. Tresser, *Phys. Rev. Lett.* **72**, 80 (1994).
- [99] D. MacKernan, Ph.D. thesis, Université Libre de Bruxelles, Faculté des Sciences, Service de Chimie-Physique, 1997 (unpublished).
- [100] T. Berlin and M. Kac, *Phys. Rev. A* **86**, 821 (1952).
- [101] G. Kowalewski, *Einführung in die Determinantentheorie*, 4th ed. (de Gruyter, Berlin, 1954).
- [102] P. Davis, *Circulant matrices* (Wiley Interscience Publ., New York, 1979).
- [103] R. Zurmühl and S. Falk, *Matrizen und ihre Anwendungen*, 5th ed. (Springer, Berlin, 1984), Vol. 1.
- [104] R. Klages (unpublished).
- [105] A. Rechester and R. White, *Phys. Rev. Lett.* **44**, 1586 (1980).
- [106] A. Rechester, M. Rosenbluth, and R. White, *Phys. Rev. A* **23**, 2664 (1981).
- [107] I. Dana, N. Murray, and I. Percival, *Phys. Rev. Lett.* **65**, 1693 (1989).
- [108] I. Dana, *Physica D* **39**, 205 (1989).
- [109] P. Leboeuf, preprint, *chao-dyn/9611017* (1996).
- [110] P. Gaspard, *Phys. Lett. A* **168**, 13 (1992).
- [111] W. de Melo and S. van Strien, *One-dimensional dynamics*, Vol. 25 of *Ergebnisse der Mathematik und ihrer Grenzgebiete, 3.Folge* (Springer, Berlin, 1993).
- [112] An analogous *dynamical reduction* of the chain of boxes, which is based on a distinction between internal box motion and external jumps between boxes [32,41,76], leads to another method for computing diffusion coefficients [58,120].
- [113] Standard root-finding procedures of software packages like NAG and IMSL require the respective functions to be continuous. Thus, for the problem here a grid method has been developed, where $\tilde{M}_a^n(\epsilon) - \delta$, cf. Eq. (36), has been discretized and where it has been checked whether a value of this difference is close to zero by varying ϵ . Within a range of some CPU seconds of computing time on workstations like, e.g., SUN SPARC's, a precision of up to eight digits behind the decimal point could easily be obtained.
- [114] Numerical evidence has been obtained from plots which show Markov partition values of the slope with respect to their iteration numbers n : It could be observed that for the three series of Markov partition values defined above, the number of Markov partitions in a certain range of the slope increases like a power law with respect to the iteration number n and that the Markov partition values of the slope seem to cover the real line densely, although not uniformly, in certain regions of the slope, with respect to increasing the iteration number n .
- [115] R. Beam and R. Warming, Technical Memorandum 103900, NASA Ames Research Center, Moffett Field, California (unpublished).
- [116] W. Trench, *Lin. Alg. Appl.* **64**, 199 (1985).
- [117] For example, for slope $a \simeq 6.8729834$, chainlength $L = 100$ and periodic boundary conditions, one finds numerically a considerable number of eigenvalues less than zero, and the smallest numerical eigenvalue is less than -1 , whereas analytical solutions give only a few eigenvalues less than zero, and the smallest one is only slightly below zero and clearly greater than -1 . For the computations discussed here, the versions IMSL 1.1 and 2.0 and NAG MK14B and 15A have

been used.

- [118] L. Reichel and L. Trefethen, *Lin. Alg. Appl.* **162-164**, 153 (1992).
- [119] E. Basor and K. Morrison, *Lin. Alg. Appl.* **202**, 129 (1994).
- [120] R. Klages, J. R. Dorfman, and P. Gaspard (unpublished).
- [121] J. Groeneveld (priv. commun.).
- [122] B. Mandelbrot, *The Fractal Geometry of Nature* (W.H. Freeman and Company, San Francisco, 1982).
- [123] S. Tasaki, I. Antoniou, and Z. Suchanecki, *Phys. Lett. A* **179**, 97 (1993).
- [124] R. MacKay, J. Meiss, and I. Percival, *Physica D* **13**, 55 (1984).
- [125] Q. Chen and J. Meiss, *Nonlinearity* **39**, 347 (1989).
- [126] Q. Chen *et al.*, *Physica D* **46**, 217 (1990).
- [127] J. Meiss, *Rev. Mod. Phys.* **64**, 795 (1992).
- [128] The more precise values are $a \simeq 2.41421/D(a) \simeq 0.10358$, $a \simeq 2.41645/D(a) \simeq 0.10493$; and for a maximum of second order, e.g., $a \simeq 2.20557/D(a) \simeq 0.04737$, $a \simeq 2.20724/D(a) \simeq 0.04744$.
- [129] C. Dellago and R. Klages (unpublished).
- [130] G. Gallavotti and E. Cohen, *Phys Rev Lett* **74**, 2694 (1995), 0031-9007.
- [131] G. Gallavotti and E. Cohen, *J Statist Phys* **80**, 931 (1995), 0022-4715.
- [132] D. Weiss *et al.*, *Phys. Rev. Lett.* **66**, 2790 (1991).
- [133] D. Weiss, G. Luetjering, and K. Richter, *Chaos Soliton Fractal* **8**, 1337 (1997), 0960-0779.
- [134] T. Geisel *et al.*, *Phys. Rev. Lett.* **64**, 1581 (1990).
- [135] M. Fließner, G. J. O. Schmidt, and H. Spohn, *Phys. Rev. E* **53**, 5690 (1996).
- [136] P. Haenggi and R. Bartussek, in *Nonlinear physics of complex systems - current status and future trends, Springer-Series 'Lecture notes in physics'*, edited by J. Parisi, S. C. Müller, and W. Zimmermann (Springer, Berlin, 1996).
- [137] P. Jung, J. G. Kissner, and P. Haenggi, *Phys. Rev. Lett.* **76**, 3436 (1996).
- [138] P. Jung (priv. commun.).
- [139] G. Radons, *Phys. Rev. Lett.* **77**, 4748 (1996).
- [140] F. Gantmacher, *Matrizenrechnung*, 3rd ed. (VEB Deutscher Verlag der Wissenschaften, Berlin, 1971), Vol. 2.

i	0	1	2	3	4
$s_a(i)$	3.902	3.423	3.186	3.079	3.033
$s_D(i)$	1.128	1.510	1.721	1.892	2.038

TABLE I. Scaling factors for the initial region $2 \leq a \leq 3$ of the parameter-dependent diffusion coefficient $D(a)$ (see text).

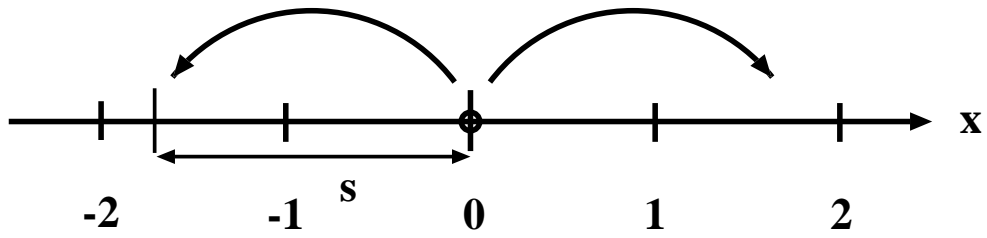


FIG. 1. Sketch of a simple one-dimensional random walk model on the real line, in contrast to deterministic dynamics.

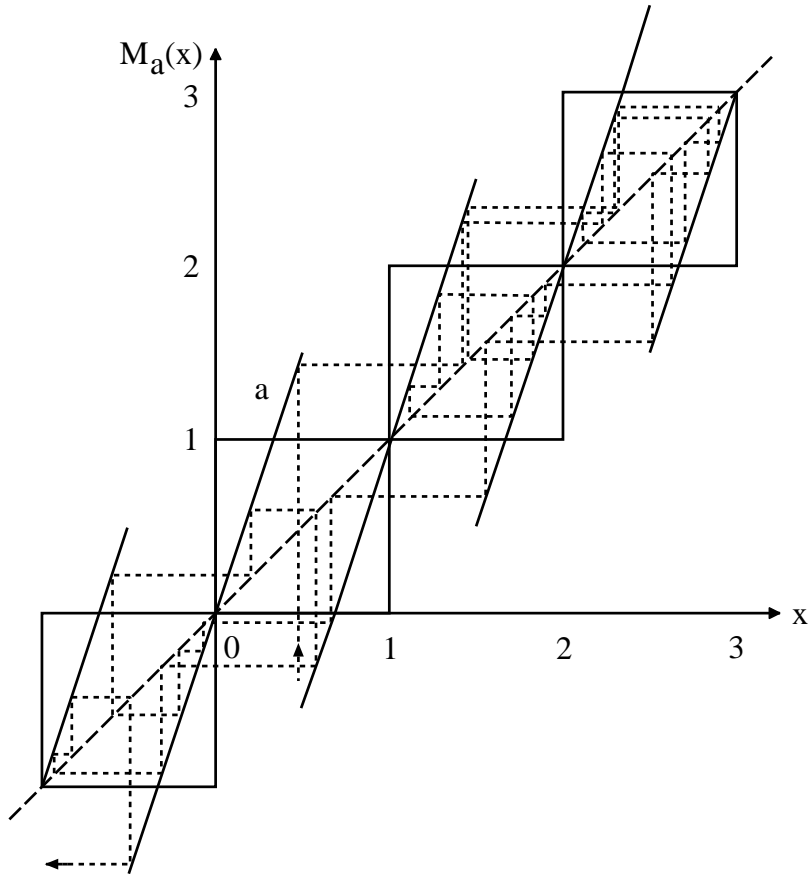


FIG. 2. Illustration of a simple model of deterministic diffusion, see the dynamical system map \mathcal{L} , Eqs.(3) to (6), for the particular slope $a = 3$. The dashed line refers to the orbit of a moving particle. Its initial condition is indicated by a black arrow close to the x -axis. The particle moves under the action of the one-dimensional piecewise linear map shown in the figure by jumping from box to box.

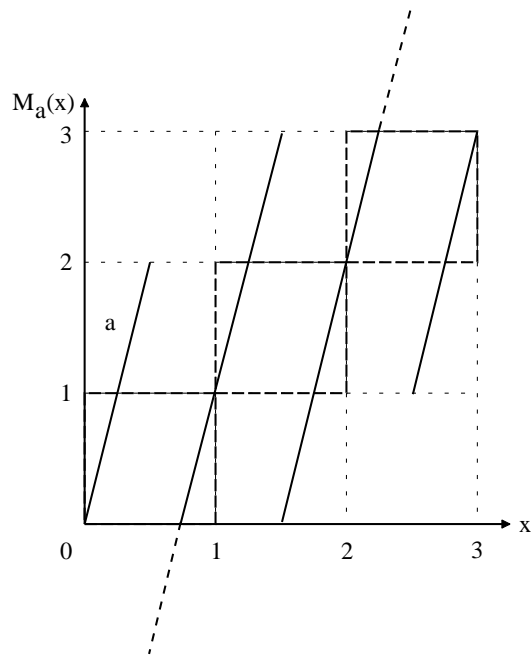


FIG. 3. Partition of map \mathcal{L} at slope $a = 4$ (dashed grid).

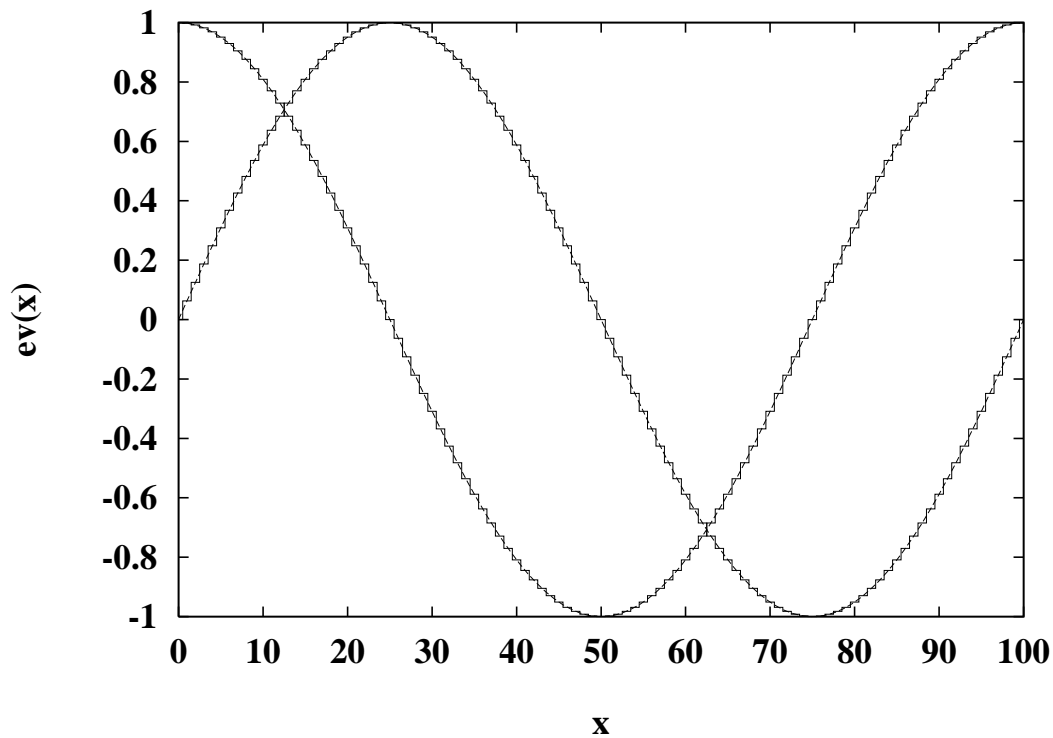


FIG. 4. The two second largest eigenmodes of map \mathcal{L} , chainlength $L = 100$, for slope $a = 3$ with periodic boundary conditions. The eigenmodes exhibit a step-like fine structure and differ by a phase shift. In comparison, the respective two eigenmodes obtained from solving the diffusion equation Eq.(7) have been included as dashed lines. They are almost indistinguishable from the map eigenmodes.

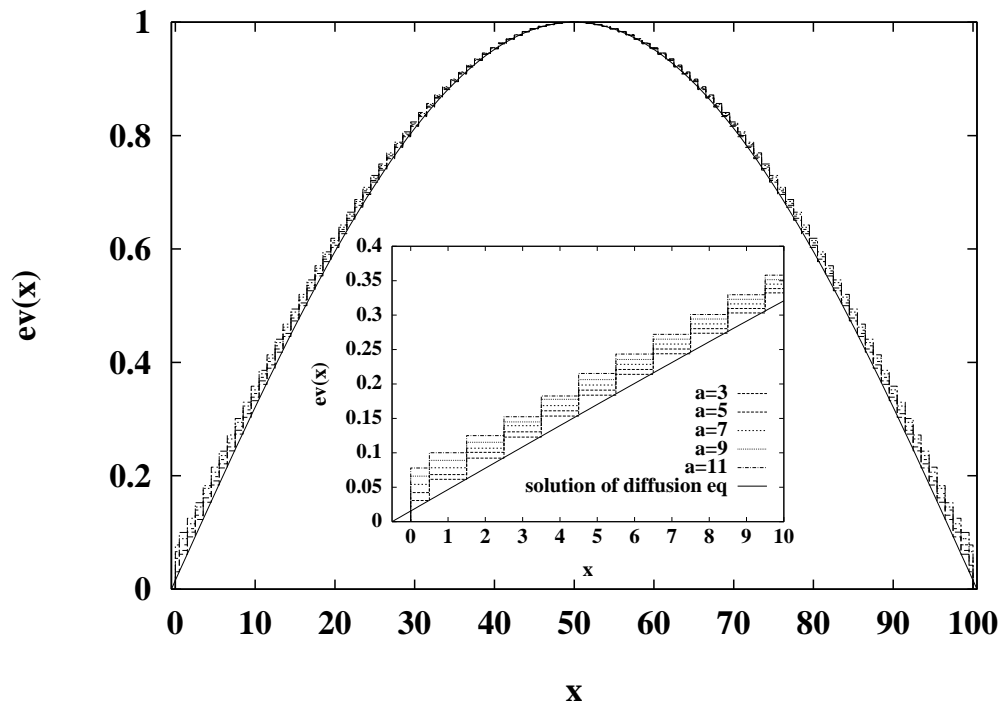


FIG. 5. Largest eigenmodes of map \mathcal{L} for odd integer values of the slope a with absorbing boundary conditions and comparison to the largest eigenmode of the diffusion equation Eq.(7). The inset is a magnification of the region around $x = 0$.

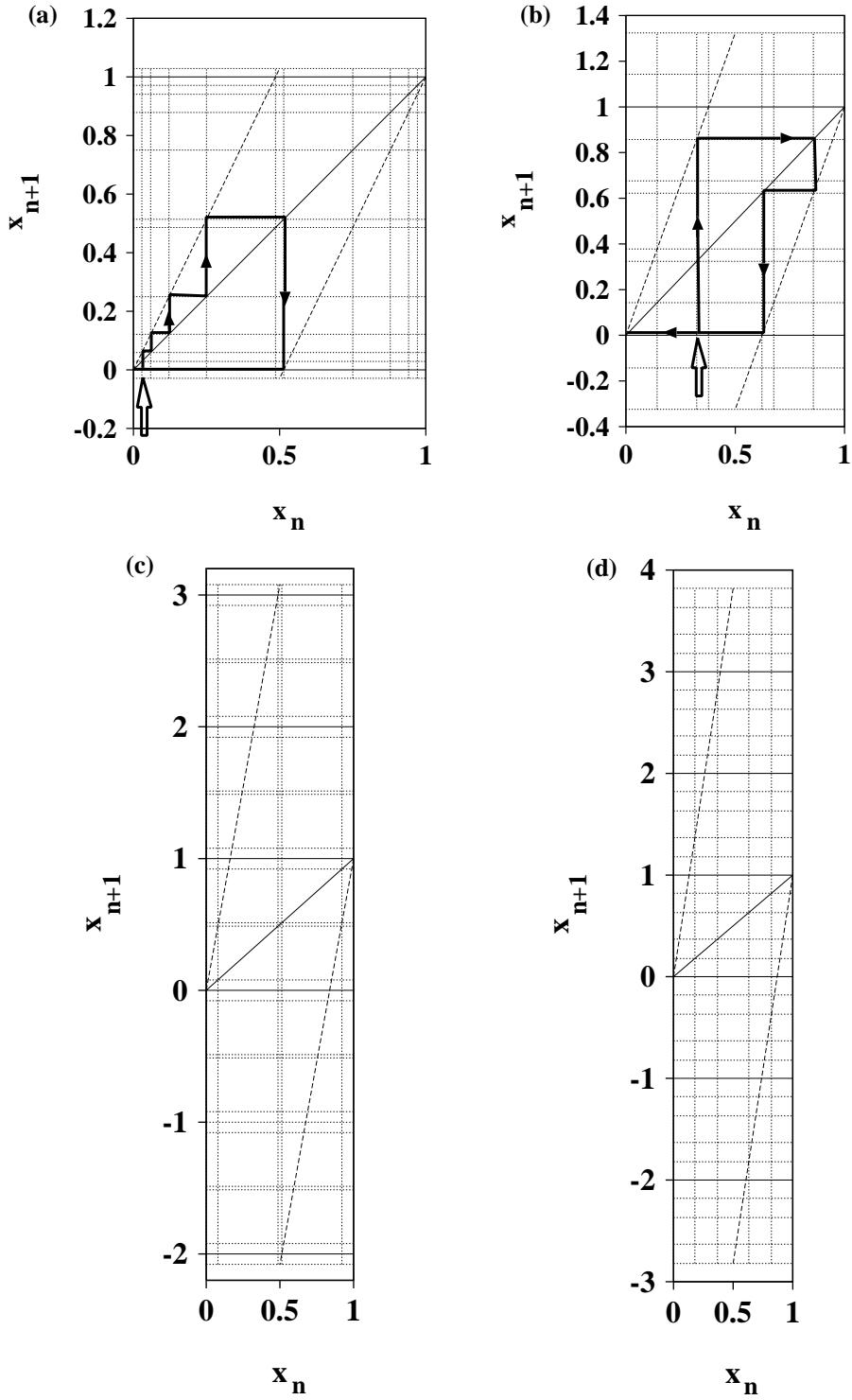


FIG. 6. Four examples of non-trivial Markov partitions of map \mathcal{L} at different values of the slope. Diagram (a) is for the slope $a \simeq 2.057$, (b) for $a \simeq 2.648$, (c) for $a \simeq 6.158$ and (d) for $a = 7.641$. In (a) and (b) the bold black lines with the arrows show the generating orbits of the partitions, that is, the orbits which define the single partition points (see text). The two large arrows below the orbits indicate the respective initial positions for the generating orbits.

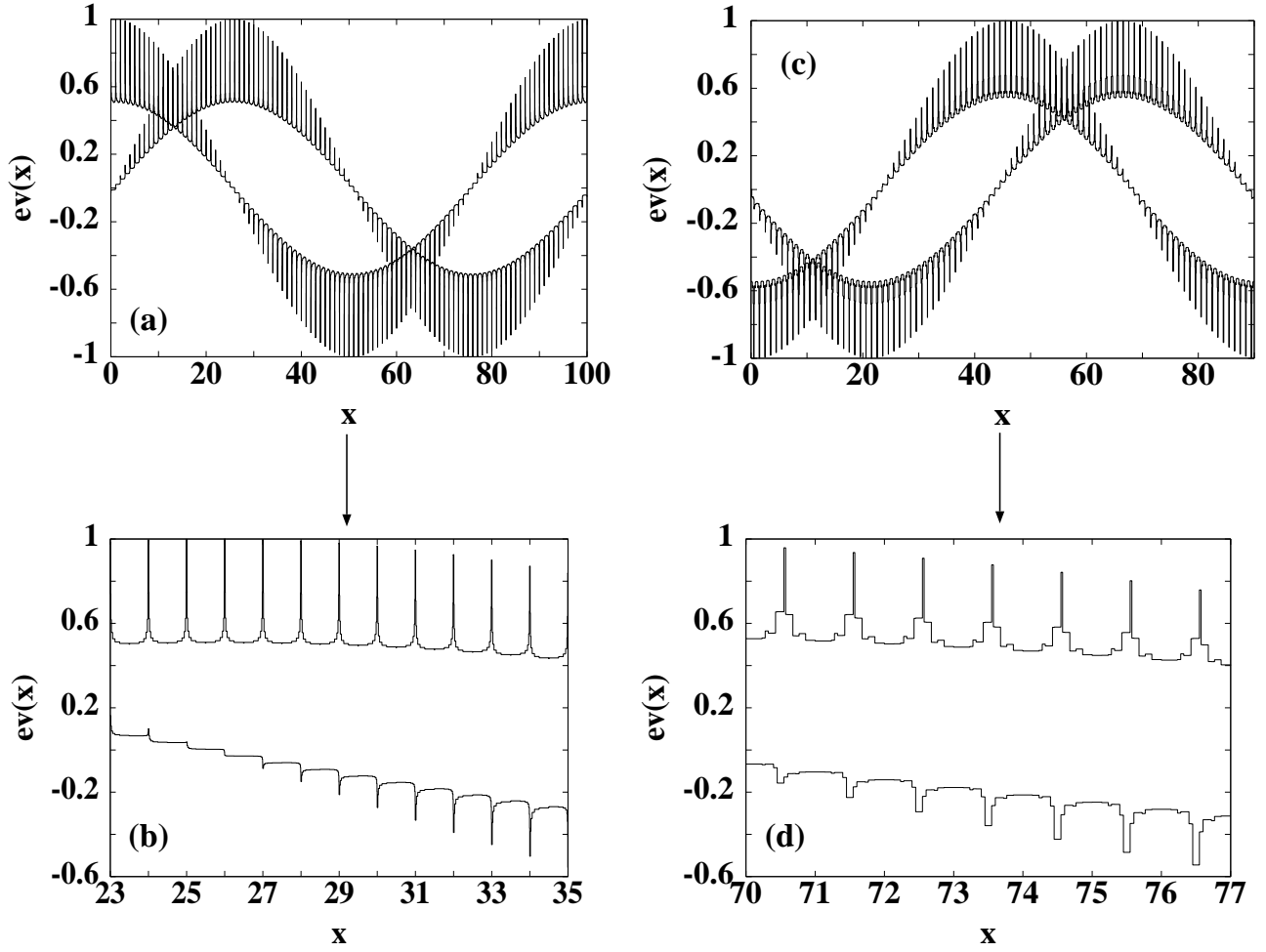


FIG. 7. Second largest eigenmodes of map \mathcal{L} at two non-trivial Markov partition values of the slope with periodic boundary conditions: full modes and magnifications of their fine structures. For both parameter values there are two largest eigenmodes which differ by a phase shift. Diagrams (a) and (b) are for slope $a = 3.0027$, chainlength $L = 100$, (c) and (d) for $a = 2.0148$, chainlength $L = 90$.

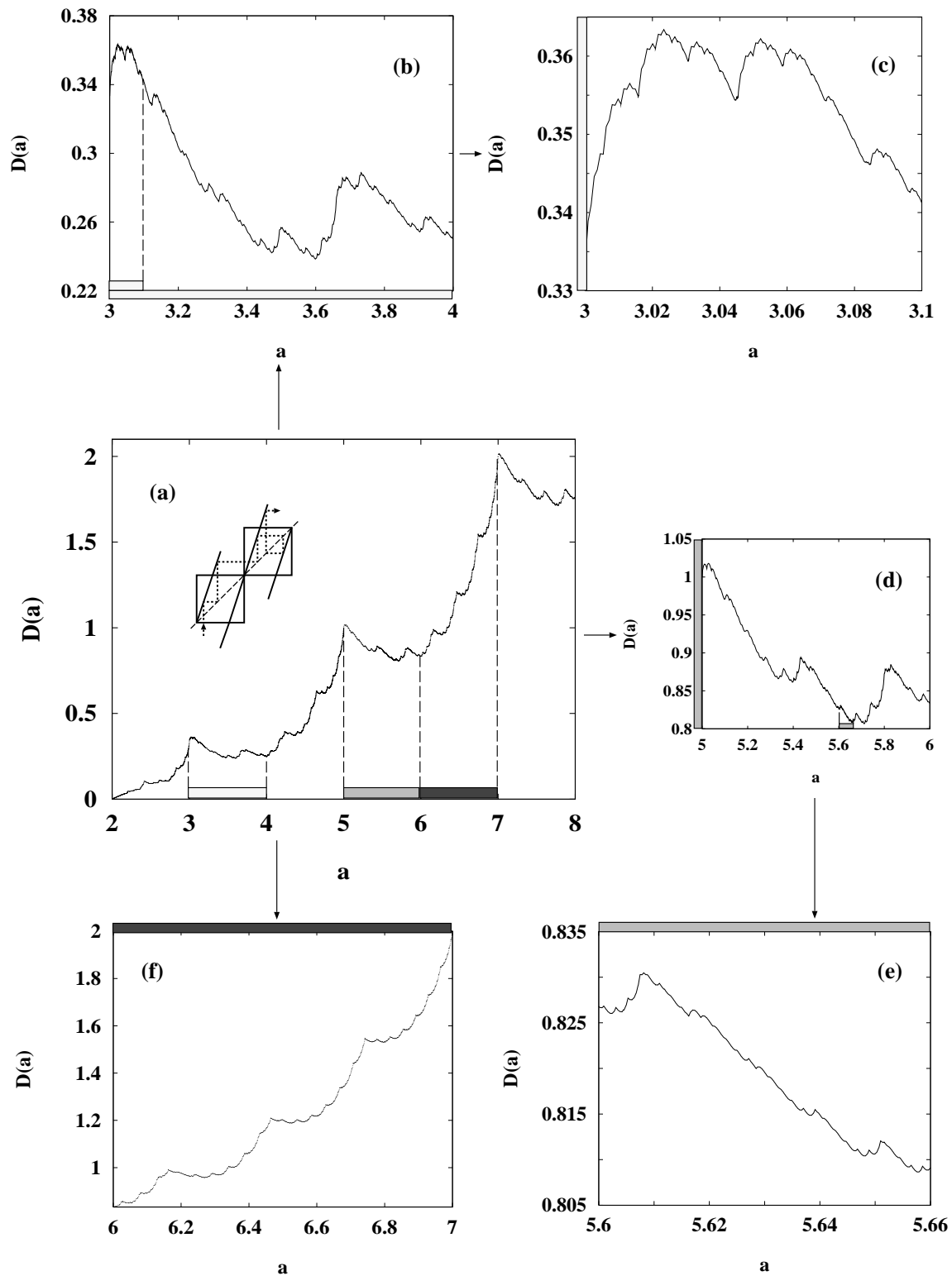


FIG. 8. Parameter-dependent diffusion coefficient $D(a)$ of map \mathcal{L} with some blowups. In graph (b)-(e), the dots are connected with lines. The number of data points is 7,908 for (a), 1,078 for (b), 476 for (c), 1,674 for (d), 530 for (e) and 1,375 for (f).

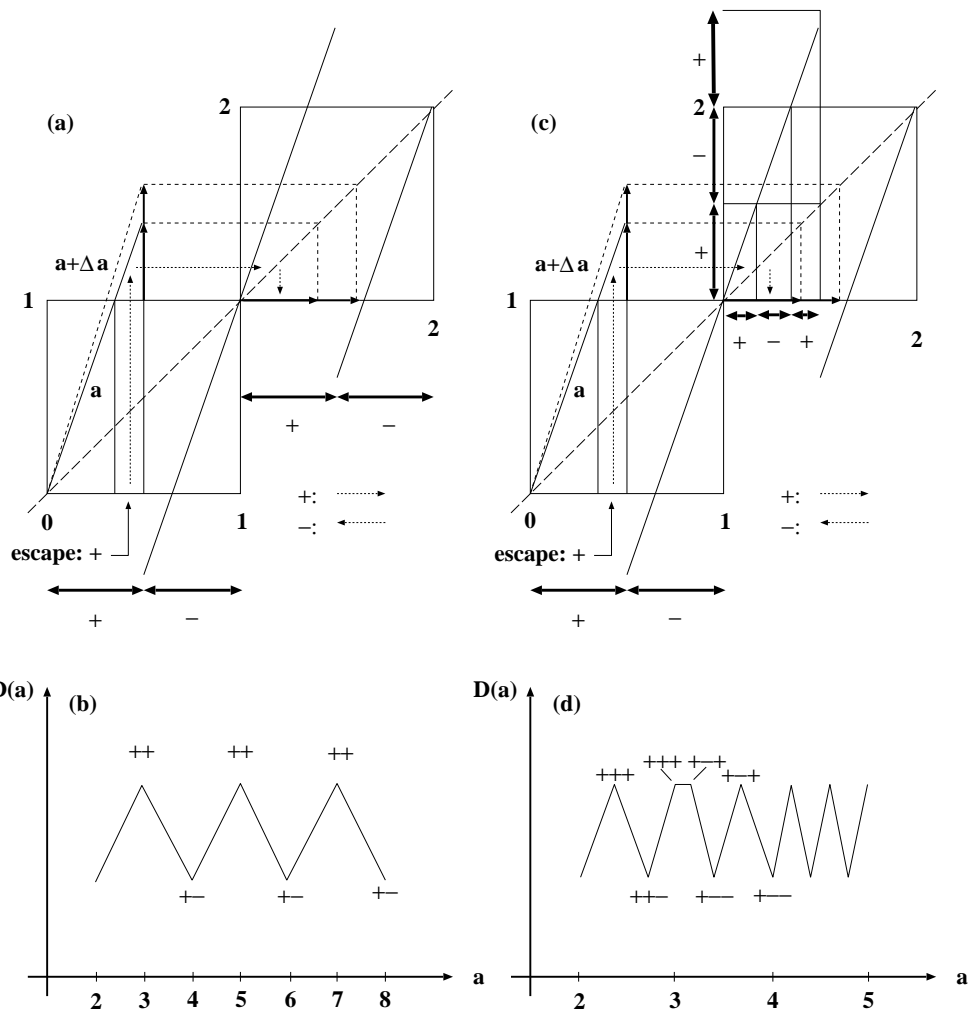


FIG. 9. First qualitative approach to understand the structure of the parameter-dependent diffusion coefficient $D(a)$, denoted as plus-minus method (see text). The variation of the microscopic scattering process via changing the slope a by Δa is heuristically related to variations in the strength of the diffusion coefficient. The plus (minus) signs refer to subintervals where forward (backward) scattering occurs at the next iteration of the map (particle moves to the right, or left, respectively). The qualitative argument is that the sequence of dominant forward or backward scattering by varying the parameter induces oscillations in the strength of the diffusion coefficient. Figs. (a) and (b) are for one iteration, Figs. (c) and (d) for two.

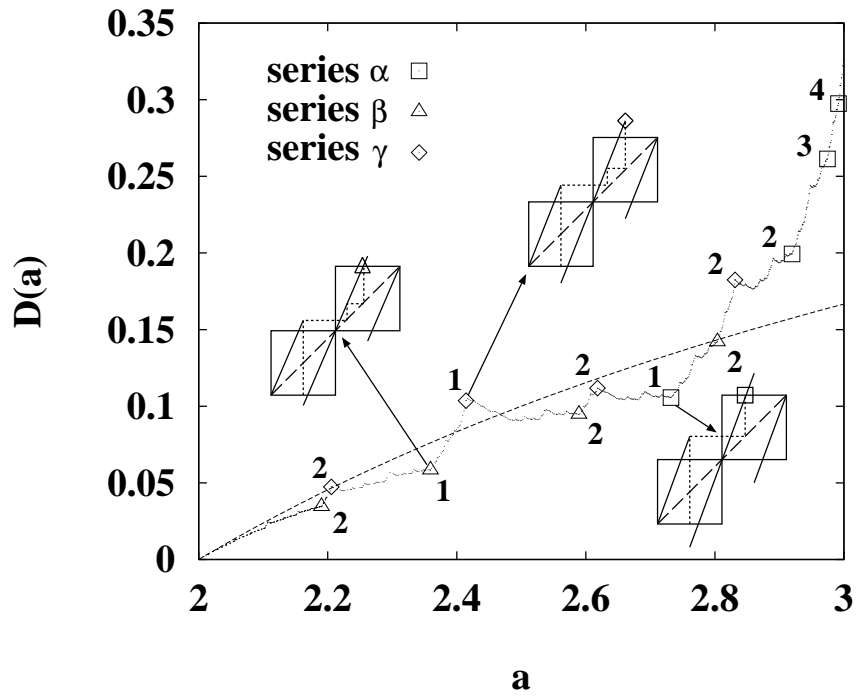


FIG. 10. Blowup of the region of slope $a \leq 3$ for map \mathcal{L} with the solution for a simple random walk model (dashed line) and labels for parameter values which are significant for “turnstile dynamics” (see text). Turnstile dynamics establishes a quantitative relation between the local maxima and minima of the parameter-dependent diffusion coefficient and the underlying microscopic chaotic scattering process. For some parameter values, the turnstile coupling is shown by pairs of boxes. The graph consists of 979 single data points.

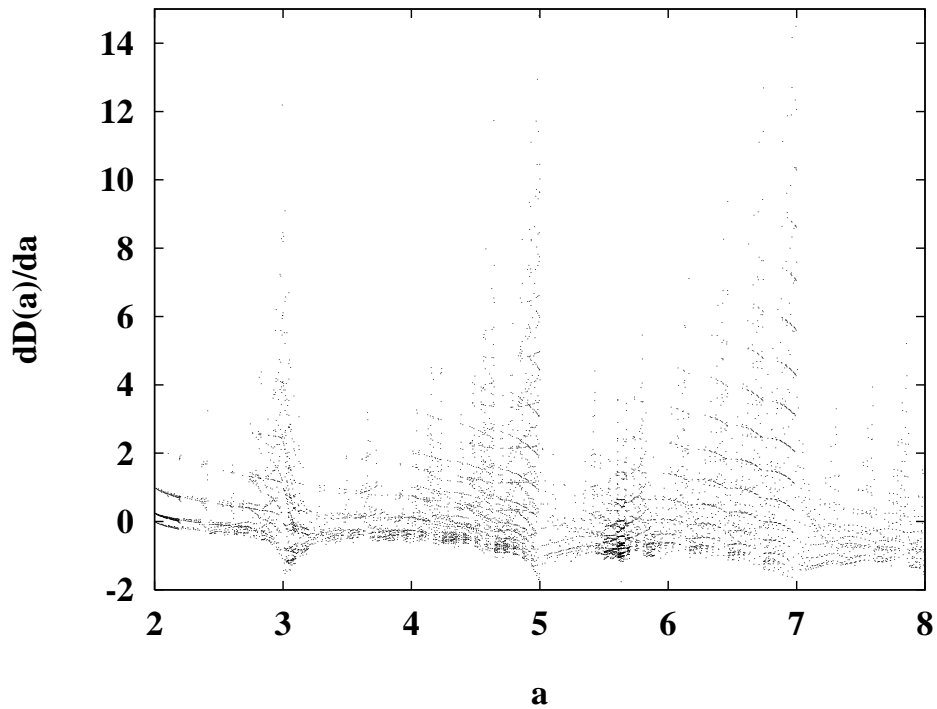


FIG. 11. Numerical derivative of the parameter-dependent diffusion coefficient $D(a)$ of map \mathcal{L} with respect to the slope a .

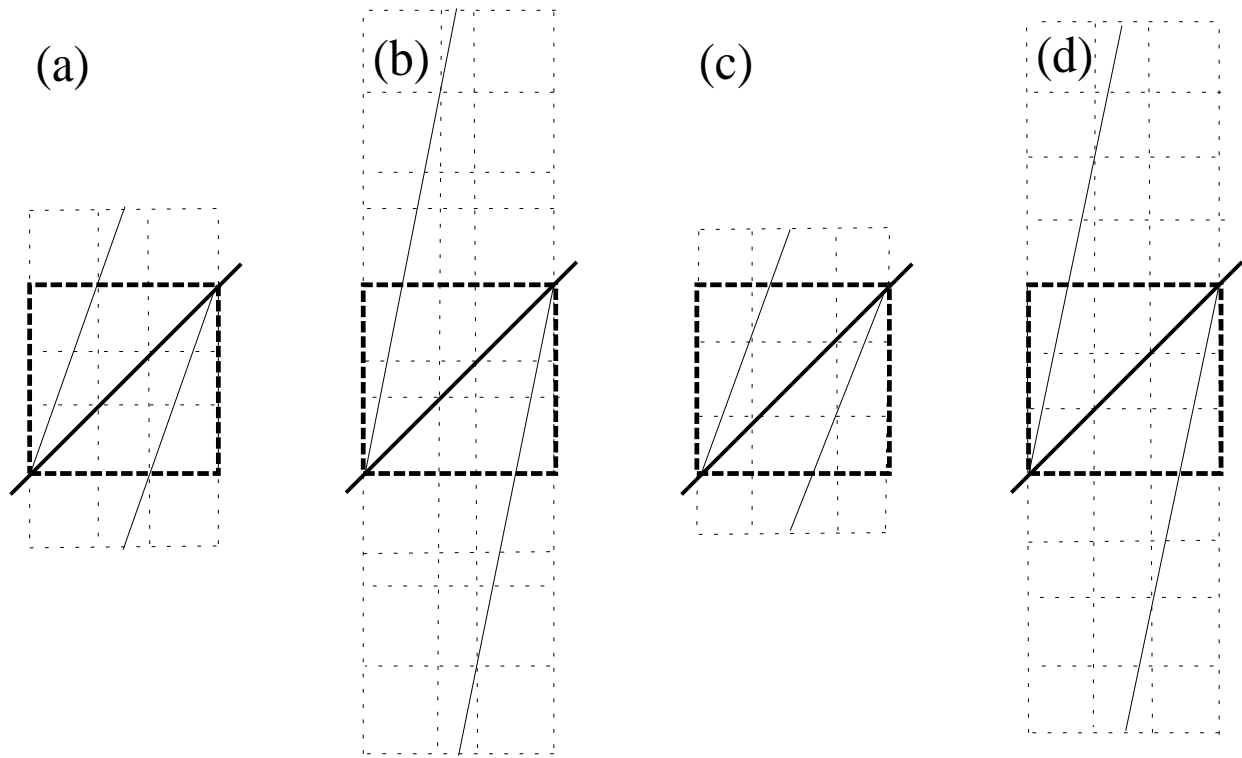


FIG. 12. Markov partitions for map \mathcal{L} at values of the slope where the diffusion coefficients are computed analytically. (a) is for slope $a \simeq 2.73205$, (b) for $a \simeq 4.82843$, (c) for $a \simeq 2.56155$ and (d) for $a \simeq 4.70156$.